A Model for Predicting Indoor Signal Levels

of Satellite Transmitted Signals

by

Matthew Aprea

Thesis submitted to the Faculty of the

Virginia Polytechnic Institute and State University

in partial fulfillment of the requirements for the degree of

Master of Science

in

Electrical Engineering

APPROVED:

Dr. Charles W. Bostian, Chairman

Dr. Brian D. Woerner

Dr. Warren L. Stutzman

August 7, 1995

Blacksburg, Virginia

A Model for Predicting Indoor Signal Levels

of Satellite Transmitted Signals

by

Matthew Aprea

Dr. Charles W. Bostian, Chairman

Electrical Engineering

(ABSTRACT)

Several possible approaches to creating a model for predicting satellite signal levels inside buildings are examined. These models make use of resonant cavity modes and vector ray addition. The cavity mode approach yields inconclusive results because of a problem with uniqueness, there are too many potential modes and no obvious way to decide between them. The ray model uses vector representation. It tracks changes, and combines rays at the receiver. Signal levels are normalized to free space values. An algorithm for the construction of such a model is developed and results are obtained. A three ray model, incorporating LOS, floor, and ceiling reflected rays gives reasonable agreement with experimental data. The types of information needed are the room height, the receiver height, if the receiver is in the vicinity of a window, and the elevation angle of the satellite. This model shows that a user has to move only a small distance to find an area where fading is brought to acceptable levels.

Acknowledgments

My sincere thanks and appreciation goes to Dr. Charles Bostian, whose support, and guidance made this project an enjoyable experience. I am grateful to Dr. Brian Woerner and to Dr. Warren Stutzman for their help, and for the privilege of having them as members of my committee.

I am thankful for all the friends I have made here at Virginia Tech without whose companionship and support would have made for a much less enjoyable stay.

Finally, I thank my family whose love; support and encouragement made this all possible.

Table of Contents

Table of Figures

CHAPTER 1. INTRODUCTION

1.1 Statement of the Problem

This thesis examines several possible approaches to creating a model for predicting satellite signal levels inside buildings. These models make use of resonant cavity modes and vector ray addition. In recent years the need for accurate prediction models for wireless communication technologies has become ever more important. Personal communications systems utilizing compact handsets that communicate via satellite are becoming more prevalent. Due to the relatively small size and portability of such a transmitter/receiver, users will want these units to perform reliably inside different types of structures (particularly office buildings, factories, arenas, parking garages, bridges...) as well as outdoors, in all kinds of weather. System designs will have to be very robust in order to perform under such adverse conditions. To be able to design such a system, models that can accurately predict satellite transmitted signal levels inside a building of concrete construction will have to be utilized. The Iridium system, which is expected to go on line in 1998, will provide worldwide coverage for any type of telephone transmission -- voice, data, fax, or paging. Designers, through the use of accurate propagation models and more sophisticated antenna design, have decreased the number of necessary satellites from 77 to 66 [EDN94]. Designers of communications systems will benefit from models that could predict signal levels and other pertinent characteristics, to make more efficient use of the available resources. Therefore models such as that presented here in this thesis take on a certain importance. This thesis will show that a vector addition model for prediction of signal levels will provide accurate results that can be used in system design.

1.2 Importance of Prediction Models

Models that can accurately predict the pertinent characteristics of a propagation environment can be very useful to designers of personal communication systems. More efficient system designs can be made by trading off modulation techniques, site

characteristics, and frequency use. For a satellite system, calculations of signal levels are very important to link budget calculations. Fading can occur from absorption loss, scattering, and reflection, as well as multipath interference. The power available for use in signal transmission is one of the limiting factors that dominate the design of a satellite system. Power received from a satellite can be characterized as follows:

$$P_r = EIRP + G_r - L_p - L_a - L_{ta} - L_{ra} - L_m \quad \text{[BOS86]} \qquad (1.1)$$

Where $EIRP$ = Effective isotropically radiated power [dBm].

P_r = Received power [dBm}.

G_r = Gain of receiving antenna [dB].

L_p = Path Losses [dB].

L_a = Atmospheric losses [dB].

L_{ta} = Losses from transmitting antenna [dB].

L_{ra} = Losses from receiving antenna [dB].

L_m = Losses from multipath interference [dB].

The necessary $EIRP + G_r$ is determined from calculations of losses and from the minimum P_r allowable such that the system will still work. Losses from multipath interference are primarily what will be analyzed in this thesis. Characterization of the losses will help determine how much power will have to be radiated for a satellite operating at a certain frequency or a range of frequencies.

1.3 Review of the Literature

The need for accurate prediction models has spurred a great deal of attention on the indoor propagation channel and the penetration of signals into buildings for terrestrial systems. Relatively little has been done for satellite systems.

1.3.1 In-building Communications

A great deal of research has focused on modeling radio wave propagation inside buildings. The indoor propagation channel links a receiver and a transmitter located at different places in the same building. Devasirvatham [DEV87] measured time delay spread in two dissimilar office buildings, finding that there are similarities in the worst case power delay profile even though the buildings have different structures. Therefore it is safe to assume that power delay profile depends on something more than just building structure. He also showed [DEV87J] that different positions for the transmitter (inside vs. outside) have an impact on the time delay spread; there are shorter delays for the indoor channel. In a later study Devasirvatham [DEV89] examined time delay spreads at 850 MHz and at 1.7 GHz finding that the different frequencies produce similar time delay properties. Rappaport [RAP89] reported the result of fading measurements on indoor communication channels in factory buildings at the 1300 MHz band. Spatial fading was measured to be between 20 and 30 dB below free space values when a station moved through a 1.3 m track. Bultitude [BUL87] found that the dynamic range of temporal fading was about 30 dB for factories or cluttered offices, and an approximately 17 dB range was found for open office spaces. A possible method of utilizing these results for the satellite communication problem would be to model the satellite transmission as coming from a transmitter located just inside the building wall. In other words, decrease the signal's power and adjust the phase to account properly for transmission through the buildings walls, then use the indoor propagation channel models presented in [RAP89A] to predict signal levels (see Figure 1.3.1). This approach is not attempted due to problems in characterizing the coupling of the field from outside to inside.

Lo et al. [LOT94] present a new approach to estimate the indoor radio propagation characteristics. Here a matrix based approach is used to predict power delay profile moments. Covariance in discrete frequency samples of the radio channel transfer function plus noise is calculated and the covariance matrix is constructed. The eigenvalues and consequent eigenvectors of the matrix are used to calculate the power

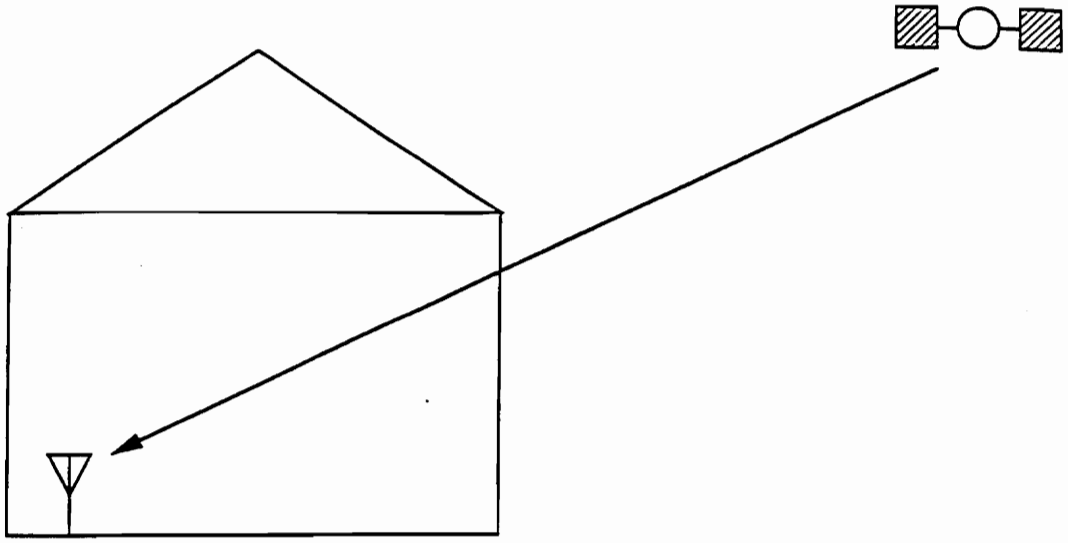

(a) Satellite transmission beamed directly to receiver

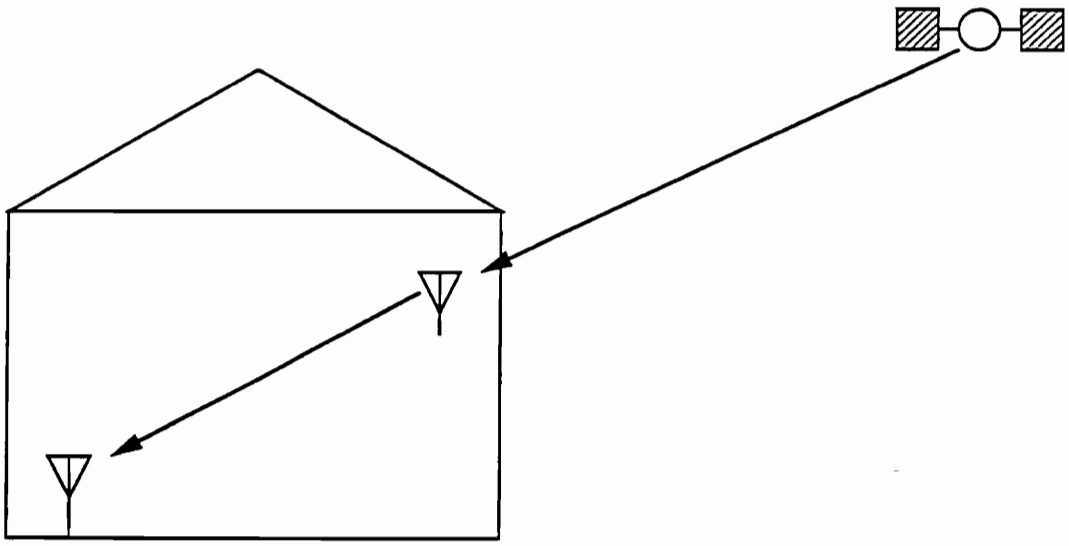

(b) Concept of Satellite transmission coupled through to indoor propagation model.

Figure 1.3.1 Possible use of indoor propagation models for satellite signal modeling.

profile moments from which the delay spread characteristics can be computed.

1.3.2 Penetration of Terrestrial Signals Into Buildings

Cox [COX83] provided measurements of 800 MHz radio transmission into buildings with metallic walls, finding that attenuation levels were greater for the metal walled buildings than for those with wooden walls. Horikoshi [HOR86] provided measurements of 1.2 GHz band radio wave penetration into concrete buildings and the affect of windows and transmitter orientation on signal levels. Turkmani [TUR88] investigated the effect of frequency, and height in a building, on penetration levels at 441, 900, and 1400 MHz. He found that penetration loss decreases as frequency and height increase. The penetration loss decreases associated with height increases were thought to be a result of a clearer path between receiver and transmitter. Molkdar [MOL91] gives a comprehensive review of a great deal of the literature available and summarizes the results for office buildings in suburban areas as follows:

The penetration loss (the difference between the received signal inside and the average of the received signal around the perimeter of the building) has been found to be between 1.5 and 36 dB. The rate of decay between 1.2 and 6.5 (m/dB), and the spatial fading is characterized as small scale Rayleigh.

1.3.3 Penetration of Satellite Signals Into Buildings

Relatively little has been done for satellite systems. The work most appropriate to this thesis is that of Wolfhard Vogel and G. W. Torrence [VOG93] at the University of Texas. Vogel used a transmitter mounted on top of a tower to simulate the path and angle of incidence of a satellite signal. A signal was then sent from this transmitter located outside, to a receiver located inside a building. He then measured signal levels inside the building and determined the time delays of the multipath components. The line of sight (LOS) was always unobstructed except by the building's walls or roof. Signal strength

was measured as a function of frequency and receiver position and a time delay profile was created. This was done for several buildings of various construction.

Vogel used a cavity backed spiral antenna that produced a right hand circularly polarized wave. The field pattern for such an antenna is found from [STU94]. The goal of this thesis is to produce computer generated predictions of signal levels that approximate those obtained experimentally by Vogel. To accurately simulate this system, it is important to assume circularly polarized waves and characterize their reflections accurately. For acceptable results, a model must keep careful track of phase information and accurately represent the receiving antenna's response to incoming signals of arbitrary polarization and direction of travel.

CHAPTER 2. PREVIOUS EXPERIMENTAL RESULTS

2.1 Introduction

In an attempt to give a more detailed description of radio wave propagation inside buildings, Vogel [VOG93] performed the following experiment. Signal strength measurements over the 700 - 1800 MHz frequency band were taken inside six different buildings. Construction varied from a small concrete walled room to a foyer of concrete construction with a large glass window to a metal shack.

2.2 Measurement Setup

The problem Vogel was presented with was to simulate a satellite's transmissions over a range of frequencies. To do this, a transmitter was mounted on a 17.9 meter tower that was in turn, mounted upon a van. This was done to simulate the elevation angle and path of a satellite transmission, and send signals to a receiver located inside a building. The antennas used were right hand circular polarized cavity backed spirals.

2.3 Measurements

Signal levels were measured while Vogel performed a frequency sweep from 700 to 1800 MHz for each of the six building types. Of particular interest are Figures 2.1.1 and 2.1.2 (Vogel's Figures 4 and 5) where the swept frequency measurements are taken for two different receiver heights (approximately 1.4 and 1.9 meters) inside the same building (labeled BRC-15) while all other factors remain the same. These figures present signal levels in dB below that expected for free space transmission. It can be seen that the deep fade troughs that are present in Figure 2.1.1, are absent in Figure 2.1.2 but fade troughs are present here at different frequencies. If one measures the distance between consecutive nulls and peaks in Figure 2.1.1, it can be seen that there is a roughly constant separation. Figure 2.1.2 also exhibits the same constancy however the separation is not as

great. Measurements for the building labeled Commons are shown in Figure 2.1.3 (Vogel's Figure 9). Deep fade troughs are present here where the LOS path is obstructed by the building. Here again, the separation between nulls or peaks is relatively constant revealing a pattern of constructive and destructive interference that changes with frequency. Figure 2.1.4 (Vogel's Figure 10) is a graph of the signal level versus frequency when the receiver is moved to a new position inside the same building. The LOS signal passes through a window and experiences relatively little attenuation and therefore dominates the signal level measurements. Thus the deep fade troughs are absent, but there is still some constancy in the separation of the consecutive nulls or peaks.

Figure 2.1.5 is the cpf of the time delay spread at one position in three of the buildings. Included are buildings labeled BRC 15-24 and Commons each of which will be examined in Chapter 6.

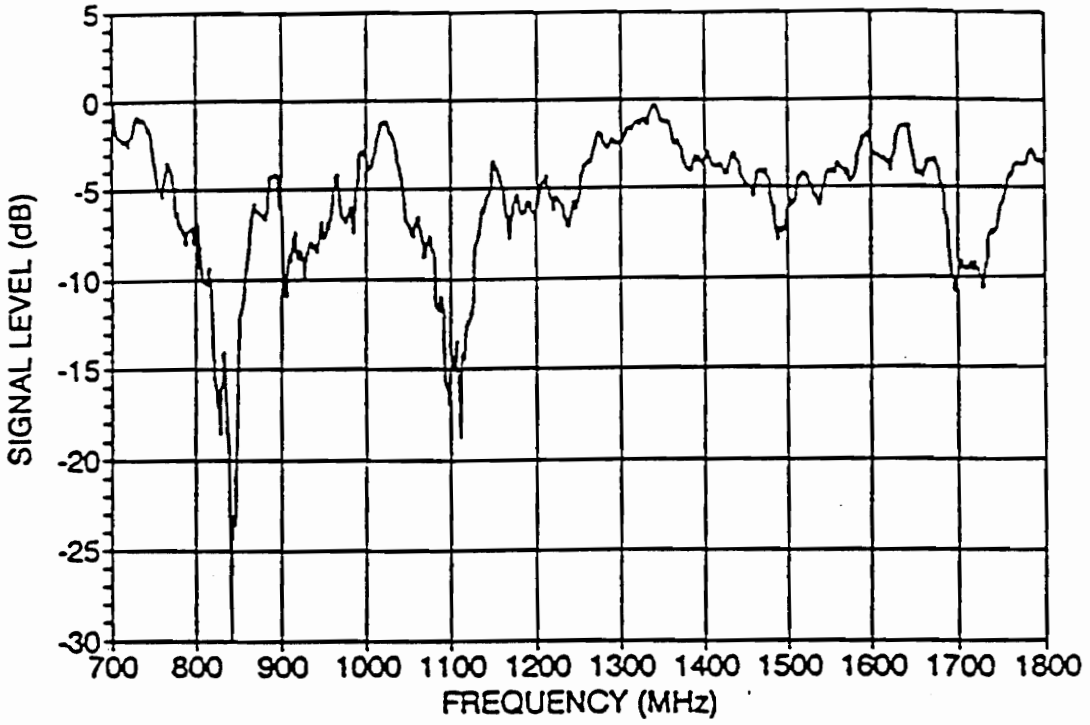

Figure 2.1.1 Vogel's Figure 4, showing signal level in dB below free space vs. frequency at a receiver height of 1.4 meters and elevation angle of 18 degrees, in building BRC 15-24. The deepest fade troughs appear near 850 and 1100 MHz. (Reprinted with permission from [VOG93].)

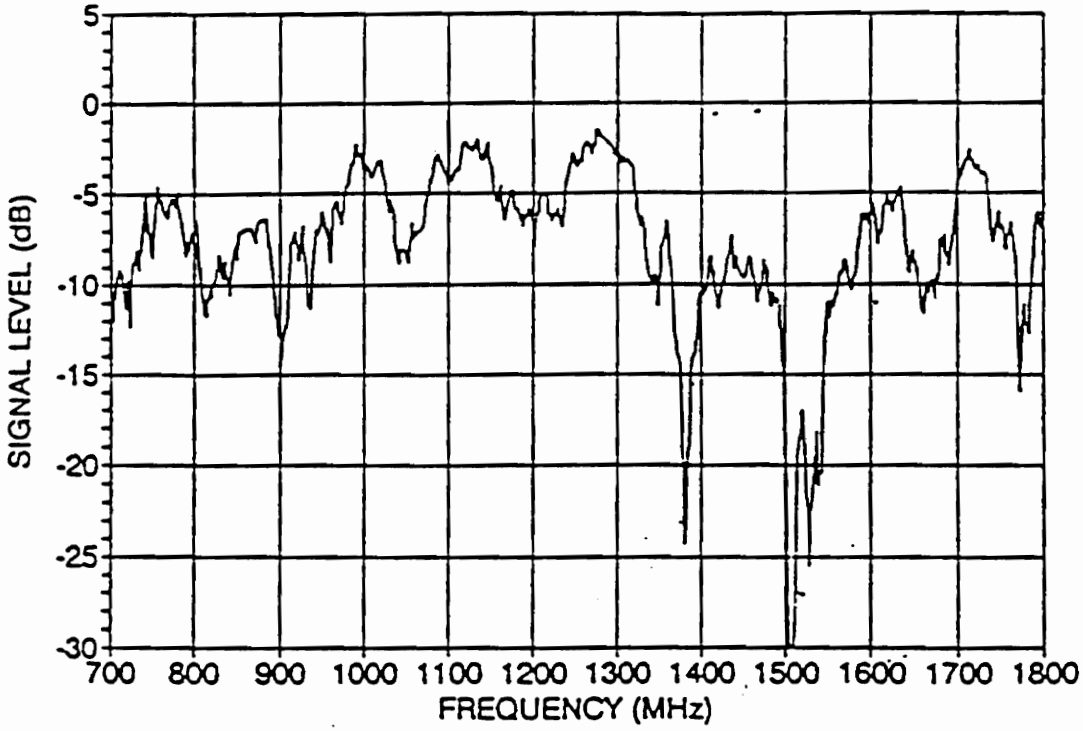

Figure 2.1.2 Vogel's Figure 5, showing signal level in dB below free space vs. frequency at a receiver height of 50 cm higher than Figure 2.1.1 and elevation angle of 18 degrees, in building BRC 15-24. The deepest fade troughs appear near 1400 and 1500 MHz. (Reprinted with permission from [VOG93].)

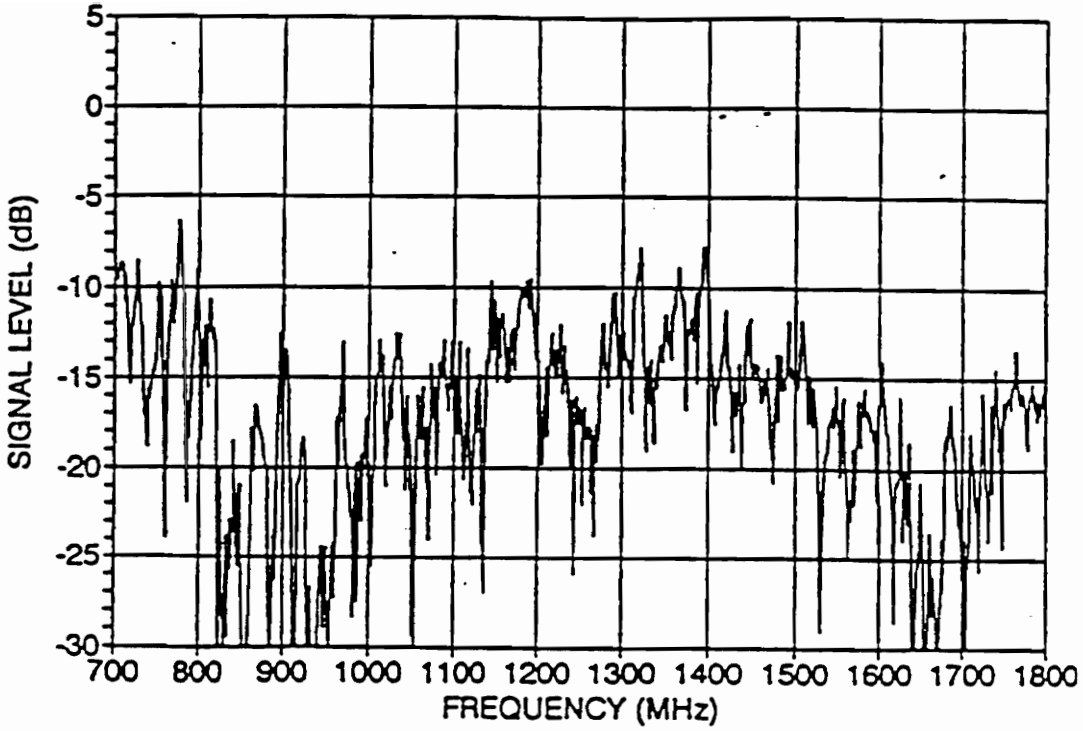

Figure 2.1.3 Vogel's Figure 9, showing signal level in dB below free space vs. frequency at a receiver height of 1.4 meters and elevation angle of 16 degrees, in building Commons. The deepest fade troughs appear near 900 and 1650 MHz. The line-of-sight penetrated the exterior concrete wall. (Reprinted with permission from [VOG93].)

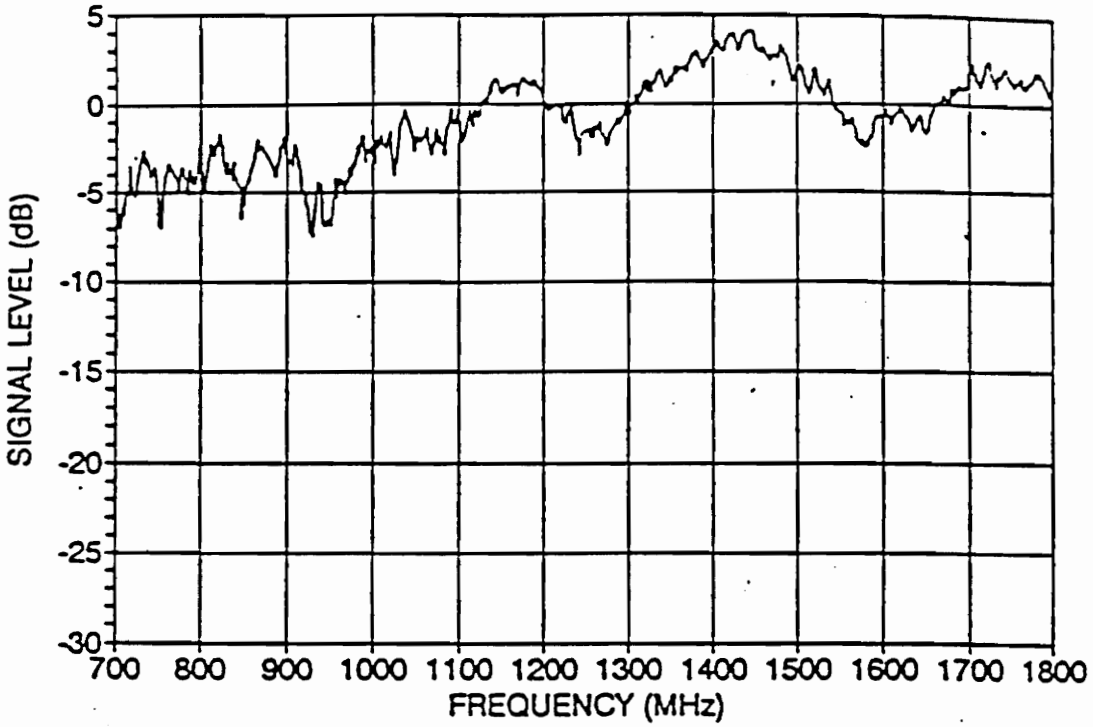

Figure 2.1.4 Vogel's Figure 10, showing signal level in dB below free space vs. frequency at a receiver height of 1.4 meters and elevation angle of 16 degrees, in building Commons. The deepest fade troughs appear near 900 and 1650 MHz. Now the line-of-sight penetrated the window. (Reprinted with permission from [VOG93].)

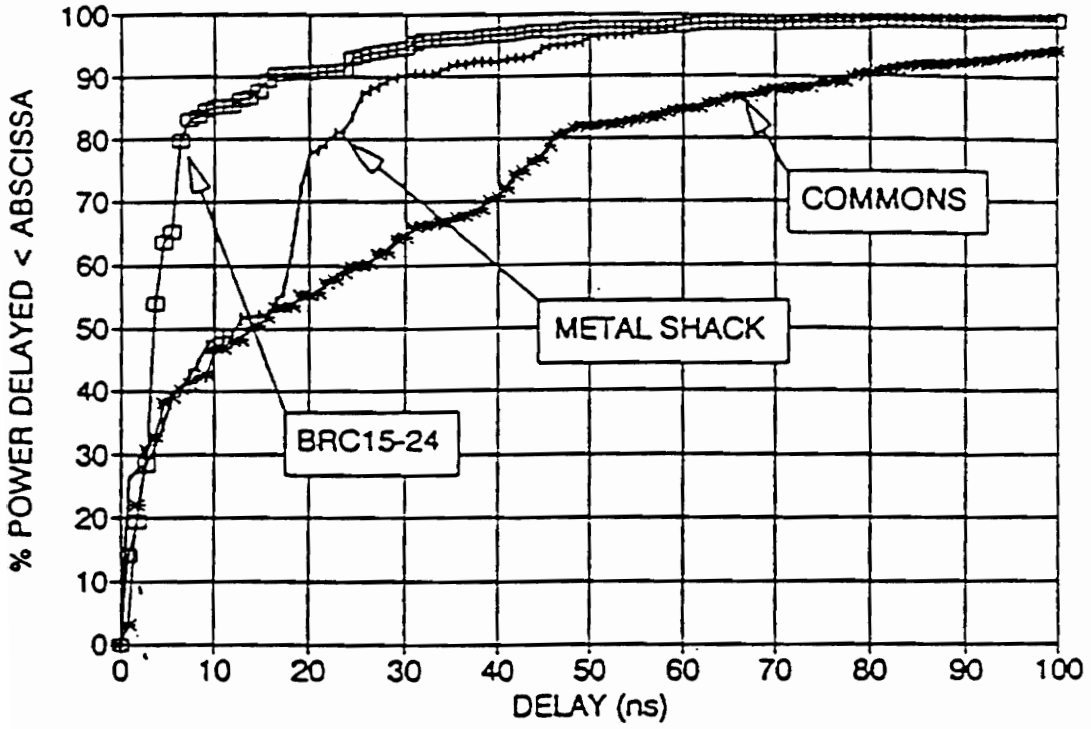

Figure 2.1.5 Vogel's Figure 12, the cpf of time delay spread at one position in three buildings. (Reprinted with permission from [VOG93].)

CHAPTER 3. POSSIBLE MODELS

3.1 Statistical Models

After collecting the data from the mock satellite setup, Vogel [VOG93] attempted to fit a statistical regression model to the data. Measurements of six buildings produced four regression coefficients for a curve that shows the percentage of positions at which the received signal is below a certain threshold. The coefficients differ for each building. Table 3.1.1 presents some of the regression coefficients derived.

Table 3.1.1 Sample regression coefficients from [VOG93]

Building	*A0*	*A1*	*B0*	*B1*
BRC 15-24	74.1	7.0	20.3	-1.2
Commons	105.7	3.1	-7.8	-.34

These coefficients are used to fit a curve to the data collected and show the percentage of positions P (%) at a given frequency (F (GHz)) which have an average received power that is below a given threshold (THR (dB below free space)). P (%) is approximated using the following relationship:

$$P = A + B*F \tag{3.1}$$

where

$$A = A0 + A1*THR \tag{3.2}$$

and

$$B = B0 + B1*THR \tag{3.3}$$

$A0, A1, B0, B1$ are found in Table 3.1.1

Figure 3.1.1 is an example of this type of curve for a sample threshold level. Furthermore two more regression coefficients are determined for a fit to the data collected of the frequency width of fade troughs for a given threshold level (dB). In other words the bandwidth over which the signal is below some threshold.

This type of modeling gives no insight into the physical phenomena within the structure. From this we only know the percentage of positions that have signal power

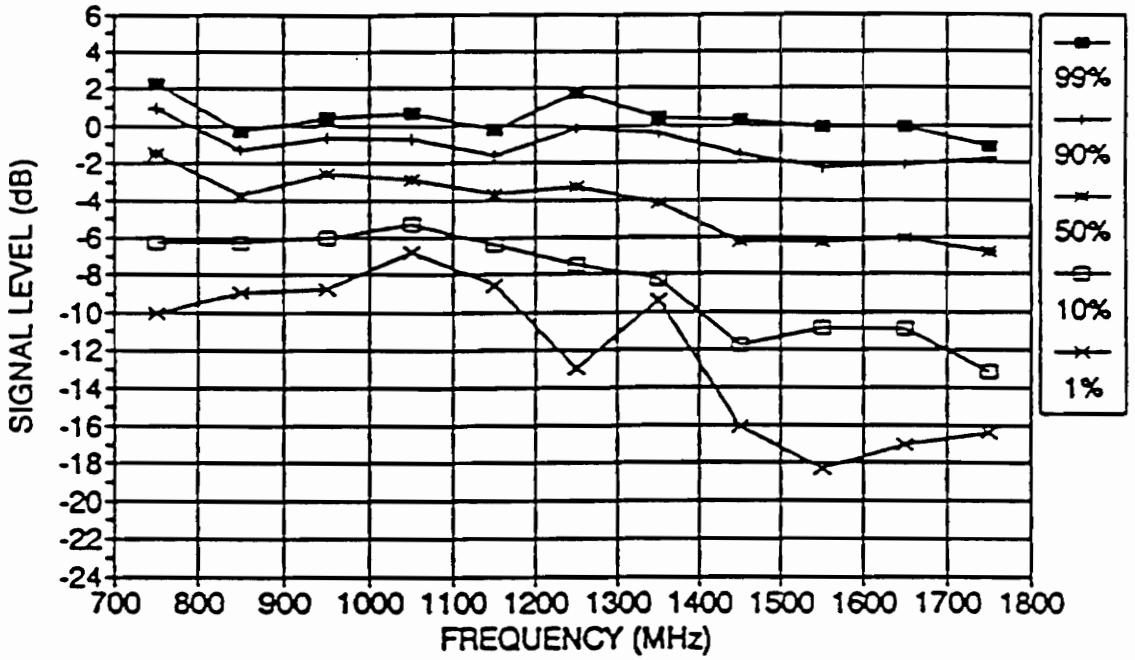

Figure 3.1.1 Vogel's Figure 16, probability contours for the signal being less than the ordinate at 99, 90, 50, 10, and 1% at the best position in the scan for building BRC 15-24. (Reprinted with permission from [VOG93].)

levels below a certain threshold level. A general increase in P can be seen as the frequency increases. This may be because the reflection coefficients of building materials typically increase with frequency. There will be less loss due to reflection which will increase the received power when the multipath components add in phase. This does not allow us to predict when and where the deep fade troughs will occur. Modeling in this manner is not general enough for prediction of characteristics of buildings in which measurements were not taken. Therefore additional models may be necessary.

3.2 Cavity Mode Models

One possible prediction tool is to model the room that contains the receiver as a cavity resonator. Reflections from floors, ceilings, and walls may create standing waves whose characteristics are well known and can be predicted. Problems that arise with this model are the different reflection and transmission coefficients of the surfaces, and the coupling from the satellite to the room. Calculations have shown that there are a great number of higher order modes that are above the cutoff frequency for rooms the size of common offices. The problem is to determine which mode is dominant. This approach is further documented in Chapter 4.

3.3 Multipath Model

As radio waves are transmitted from a satellite to a receiver on or near the surface of the Earth, surrounded by many scattering objects, as is a receiver inside a building, multipath interference poses a large problem. Many attenuated and time delayed versions of the signal reach the receiver and cause interference with the LOS path. In the cavity mode model these signals are examined as a whole (i.e., the total signal strength). Here the satellite transmission is broken up into its many multipath components and the interaction of these at the receiver is investigated. This type of modeling is examined further in Chapters 5 and 6.

4.1 Theory of Resonators

One possible way to model satellite transmissions into a building is to model the room that holds the receiver as a cavity resonator. The fields in a cavity resonator can be described by a set of equations that can be derived directly from Maxwell's equations using the boundary conditions determined by the specific geometry of the room or cavity (see Figure 4.1.1). Solving these for the phasor electric field components, a rectangular room with dimensions a, b and d, with a wave traveling in the +z direction, for TM modes yields:

$$\begin{aligned} E_x(x,y,z) &= -\frac{1}{h^2}\left(\frac{m\pi}{a}\right)\left(\frac{p\pi}{d}\right)E_0\cos\left(\frac{m\pi}{a}x\right)\sin\left(\frac{n\pi}{b}y\right)\sin\left(\frac{p\pi}{d}z\right) \\ E_y(x,y,z) &= -\frac{1}{h^2}\left(\frac{n\pi}{b}\right)\left(\frac{p\pi}{d}\right)E_0\sin\left(\frac{m\pi}{a}x\right)\cos\left(\frac{n\pi}{b}y\right)\sin\left(\frac{p\pi}{d}z\right) \quad \text{[V/m]} \quad (4.1) \\ E_z(x,y,z) &= E_0\sin\left(\frac{m\pi}{a}x\right)\sin\left(\frac{n\pi}{b}y\right)\cos\left(\frac{p\pi}{d}z\right) \end{aligned}$$

Where m, n, and p are the mode numbers $m,n,p \in 0,1,2\ldots$ corresponding to the number of half wavelengths in a given direction, E_0 is the amplitude of the incident wave, and h is:

$$h^2 = \left(\frac{m\pi}{a}\right)^2 + \left(\frac{n\pi}{b}\right)^2. \quad (4.2)$$

A mode is a standing wave pattern designated by the mode numbers m, n, and p, specific to the geometry of a cavity, whose resonant frequency can be found by the following relationship:

$$f_{m,n,p} = \frac{1}{\sqrt{\mu\varepsilon}}\sqrt{\left(\frac{m}{a}\right)^2 + \left(\frac{n}{b}\right)^2 + \left(\frac{p}{d}\right)^2} \quad \text{[Hz]} \quad (4.3)$$

where μ = permeability of the medium [H/m]

ε = permittivity of the medium [F/m]

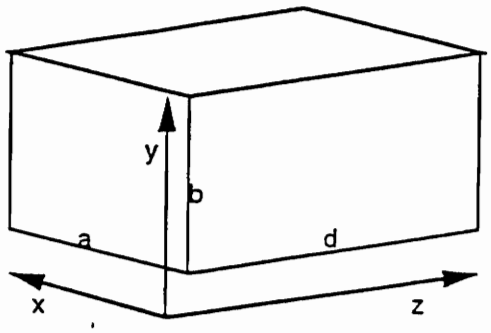

(a) Geometry of the cavity

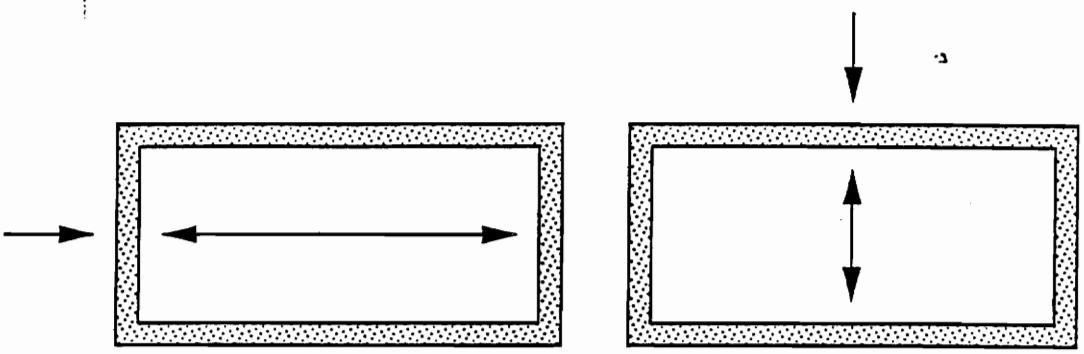

(b) Normally incident waves

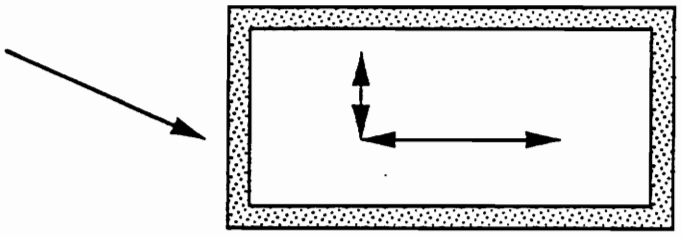

(c) Obliquely incident waves

Figure 4.1.1 Cavity resonator. (a) the directions of the axes and the dimensions of the cavity, (b) standing wave results from normally incident waves, (c) standing wave results from obliquely incident waves.

This however requires knowledge of the mode numbers m, n, and p. The direction of propagation is an arbitrary designation used for convenience. We could easily choose x, or z. We are choosing the z - axis as the direction of travel as a reference, simply for convenience. Since the ends of the chamber (normal to the z - axis) are closed, the normally incident wave reflects back on itself, and standing waves result. A plane wave traveling in the + z direction, is given by $e^{-j\beta z}$ where β is the phase constant, $\omega\sqrt{\mu\varepsilon}$ and ω is the radian frequency found by the relation $\omega = 2\pi f$. Reflection with the chamber walls results in a wave traveling in the - z direction, given as $e^{+j\beta z}$. The superposition of these two waves results in a $\cos(\beta z)$ or $\sin(\beta z)$, depending on the field component. For example, the transverse E-field components $\vec{E}_x$ and $\vec{E}_y$ must be zero at z = 0, and therefore, this results in $\sin(\beta z)$. It can be shown that the other components of the field vary as $\cos(\beta z)$.

These equations must now be adapted to depict modal activity when the waves travel in a direction that is oblique to one or more of the walls of the structure as seen in Figure 4.1.1. This can be dealt with in the following manner. First break the obliquely incident wave up into its component parts in the coordinate system made up of the structure's walls. For example an obliquely incident wave can be broken up into waves traveling in the +z direction and the +x direction at an angle θ from the z-axis in the x-z plane. Then add the vector components of each directions wave equations. The result is the following for TM modes:

$$
\begin{aligned}
E_x(x,y,z) &= \left[1-\frac{1}{h^2}\left(\frac{m\pi}{a}\right)\left(\frac{p\pi}{d}\right)\right]E_0\cos\left(\frac{m\pi}{a}x\right)\sin\left(\frac{n\pi}{b}y\right)\sin\left(\frac{p\pi}{d}z\right)\sin\theta \\
E_y(x,y,z) &= -\frac{1}{h^2}\left(\frac{n\pi}{b}\right)\left[\frac{p\pi}{d}+\frac{m\pi}{a}\right]E_0\sin\left(\frac{m\pi}{a}x\right)\cos\left(\frac{n\pi}{b}y\right)\sin\left(\frac{p\pi}{d}z\right) \qquad (4.4) \\
E_z(x,y,z) &= \left[1-\frac{1}{h^2}\left(\frac{m\pi}{a}\right)\left(\frac{p\pi}{d}\right)\right]E_0\sin\left(\frac{m\pi}{a}x\right)\sin\left(\frac{n\pi}{b}y\right)\cos\left(\frac{p\pi}{d}z\right)\cos\theta
\end{aligned}
$$

For a wave obliquely incident on all three surfaces, the following equations can be used where θ is as above and ϕ is the angle between the direction of travel and the x-z plane:

$$
\begin{aligned}
E_x(x,y,z) &= \left[1-\frac{1}{h^2}\left(\frac{m\pi}{a}\right)\left(\frac{n\pi}{b}+\frac{p\pi}{d}\right)\right]E_0\cos\left(\frac{m\pi}{a}x\right)\sin\left(\frac{n\pi}{b}y\right)\sin\left(\frac{p\pi}{d}z\right)\sin\theta\cos\phi \\
E_y(x,y,z) &= \left[1-\frac{1}{h^2}\left(\frac{n\pi}{b}\right)\left(\frac{p\pi}{d}+\frac{m\pi}{a}\right)\right]E_0\sin\left(\frac{m\pi}{a}x\right)\cos\left(\frac{n\pi}{b}y\right)\sin\left(\frac{p\pi}{d}z\right)\sin\phi \\
E_z(x,y,z) &= \left[1-\frac{1}{h^2}\left(\frac{p\pi}{a}\right)\left(\frac{m\pi}{a}+\frac{n\pi}{b}\right)\right]E_0\sin\left(\frac{m\pi}{a}x\right)\sin\left(\frac{n\pi}{b}y\right)\cos\left(\frac{p\pi}{d}z\right)\cos\theta\cos\phi
\end{aligned}
\tag{4.5}
$$

4.2 Results

Using a procedure fully developed in Chapter 5, once the electric field inside the cavity is known, we can find the open circuit voltage V_{oc} (Equation 5.10) and can produce signal level statistics in a way compatible to Vogel. Results for the cavity mode model are inconclusive. The problem that arises is that of uniqueness; the determination of which modes are excited inside the cavity and which are the cutoff modes. In a cavity with perfectly conducting walls the only modal fields that can be excited are those whose resonant frequencies coincide with the frequency of the incident field. A room however would not have perfectly conducting walls, and each mode could ideally be present over a finite bandwidth presumably centered at its resonant frequency. While it might in theory be possible to model the field inside a room using the mode whose resonant frequency is closest to the operating frequency, in practice there is no obvious choice for realistic wavelengths and room sizes. When the modal solutions are examined none is unique. There is no useful way to represent the field inside a room by a single or even by several modes. Many modes might be present and the combination that add up to the observed field is impractically difficult to find.

CHAPTER 5. VECTOR ADDITION MODEL

5.1 Introduction

To accurately simulate the results Vogel obtained, we must use a circularly polarized wave as the signal transmitted from the satellite. Circularly polarized waves can be dissected into their vector components and placed in a Cartesian coordinate system according to the following time-domain equation:

$$\vec{E} = E_x \cos(\omega t - \beta z)\hat{x} + E_y \cos(\omega t - \beta z + \phi_t)\hat{y} \quad [\text{V/m}] \qquad (5.1)$$

where $E_x = E_y$, $\phi_t = -90^\circ$ = the phase by which the y-component lags the x-component, ω = radian frequency = $2\pi f$ $[rad/s]$, and where $\beta = \omega\sqrt{\mu\varepsilon}$ $[rad/m]$ is the phase constant. This can be thought of as the vector sum of two orthogonal linearly polarized waves with the same amplitude, out of phase by 90°. The magnitude of the total electric field is constant and only the polarization rotates at radian frequency ω.

5.2 Single Ray Model (Model 1)

Here a satellite is assumed to be in orbit somewhere above a receiver. The distance is great enough such that incoming waves can be thought of as plane waves. Model 1 is what is seen at the receiver if this satellite transmits circularly polarized waves. There are no paths to the receiver other than the line of sight (LOS) path (see Figure 5.2.1). The receiver sees only a circularly polarized waveform. Recall that the equation for the electric field of an elliptically polarized wave in the time-domain is:

$$\begin{aligned} E &= \vec{E}_x\hat{x} + \vec{E}_y\hat{y} \\ \vec{E}_x &= E_x \cos(\omega t - \beta z) \\ \vec{E}_y &= E_y \cos(\omega t - \beta z + \phi) \end{aligned} \qquad (5.2)$$

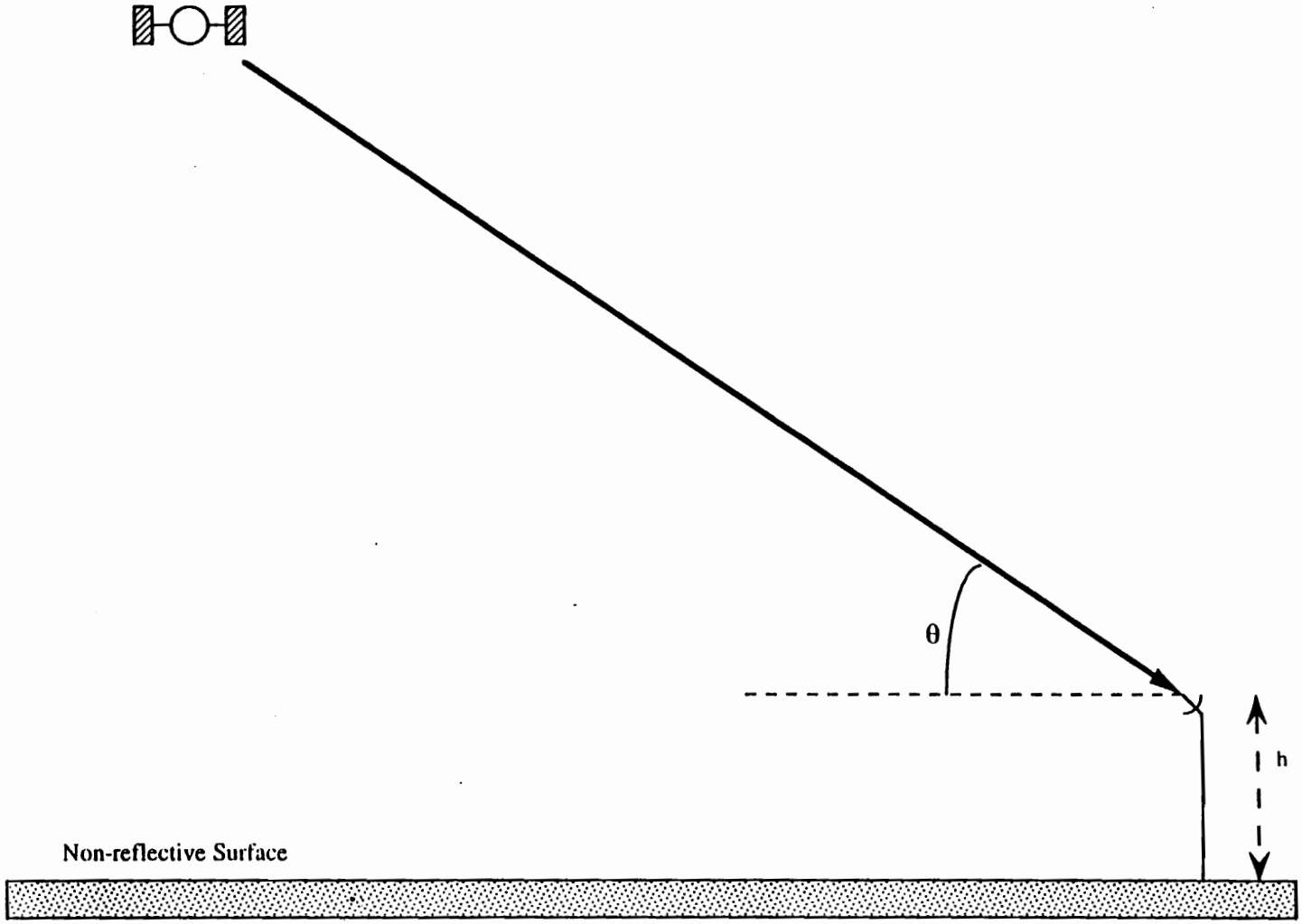

Figure 5.2.1 Single ray model. Circularly polarized ray incident on a receiver.

or in phasor form:

$$\begin{aligned} \bar{E}_x &= E_x e^{j(\omega t - \beta z)} \\ \bar{E}_y &= E_y e^{j(\omega t - \beta z + \phi)} \end{aligned} \tag{5.3}$$

If the wave is circularly polarized $E_y = E_x$, $\phi = -90°$, and $\hat{x}$ will lag $\hat{y}$ by 90°. This analysis is independent of time, so an $e^{j\omega t}$ can be factored out of the equation. The frequency information, however, is retained in this equation in the phase constant β defined earlier. The two methods by which a comparison to Vogel [VOG93] will be made are signal levels, and power delay profile. Since there is only one path (the LOS path), all the power at the receiver arrives as the single ray. Vogel measured fields with respect to free space. The model presented here calculates absolute E-field for an assumed incident value. In Section 5.3 we will show how to use this to normalize other fields with respect to free space. At this point it is necessary to look at the field structure not the exact values. With a single ray, a constant received signal level is present at the receiver, not the observed pattern of peaks and nulls

5.3 Two Ray Model (Model 2)

In Model 2 a satellite is assumed to be in orbit over a receiver located on the ground. It is at a distance great enough such that transmitted waves relatively close to one another can be said to be parallel to one another. Model 2 is intended to be a simulation of what is seen at the receiver if this satellite transmits circularly polarized waves, where one path is reflected off the ground in addition to the LOS path (see Figure 5.3.1).

The reflected path length is greater than the LOS path. To keep track of the phase in each ray, the path length difference must be calculated. Path lengths are calculated according to the following equations:

$$\begin{aligned} p_2 &= \frac{h}{\sin\theta} \quad [\text{m}] \\ p_1 &= p_2 \cos 2\theta \end{aligned} \tag{5.4}$$

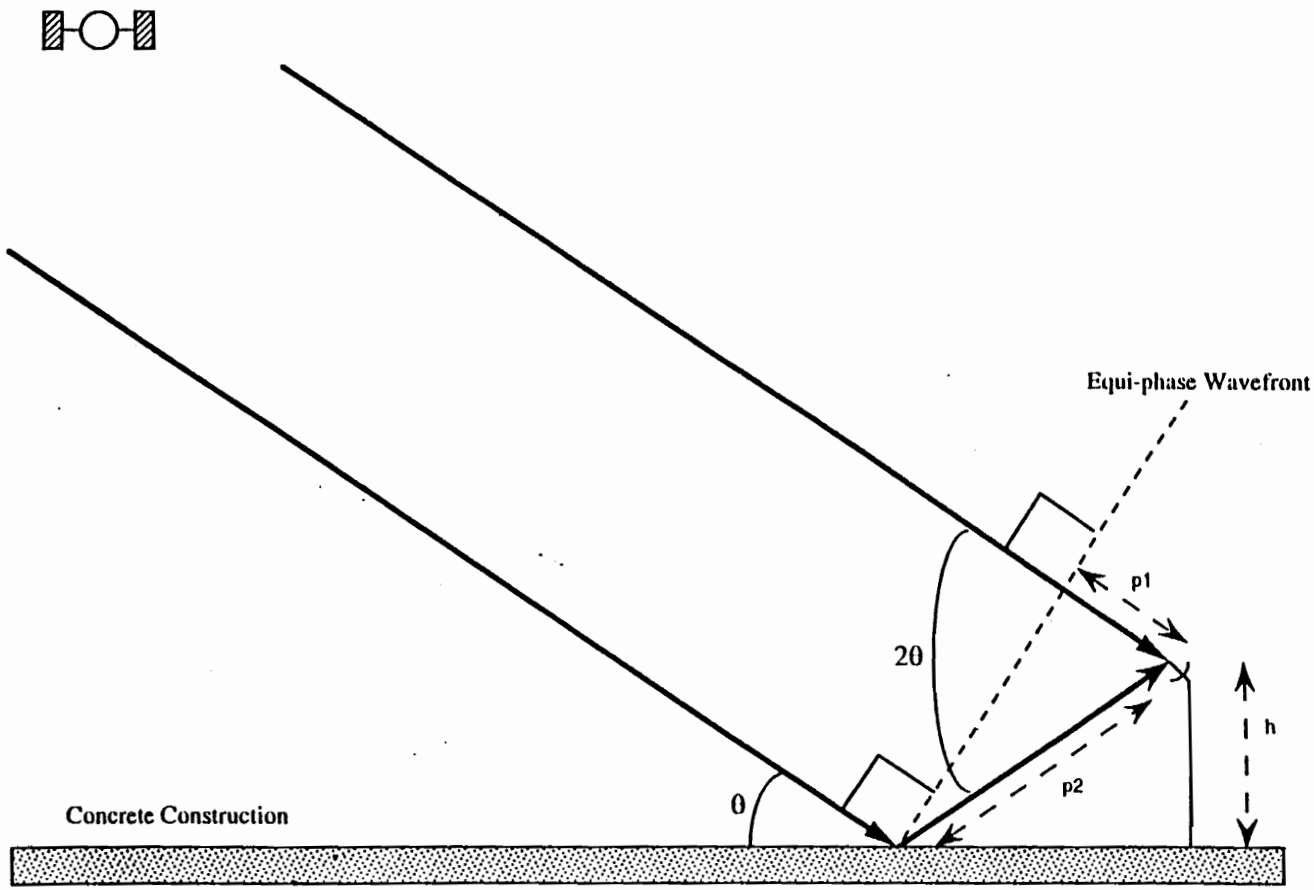

Figure 5.3.1 Two ray model. One line-of-sight ray and one reflected ray (Model 2).

where h is the height of the receiver and θ is the elevation angle of the satellite and p_1 and p_2 are the path lengths of each ray respectively after the equiphase wavefront of Figure 5.3.1. Both of the rays are circularly polarized, but because the reflected ray has a greater path length to the receiver, it arrives with a different phase from that of the LOS path.

Stutzman [STU93] and Beckmann [BEC68] show that the interaction with a reflecting plane can cause some depolarization, or for the case of circularly polarized fields cross-polarization. In other words, some of the power from the incident right hand circular polarized field is converted to a left hand circular polarization. The superposition of the two polarizations causes this reflected ray to have an elliptic polarization. In Figure 5.3.2 an electromagnetic wave is incident upon a reflecting surface with dielectric constant ε_m, and, permeability μ_m defined earlier. The plane of incidence is the plane containing the direction of propagation of the incident field and the normal to the reflecting plane. The scatter plane is the plane created by the direction of propagation of the scattered field and the normal to the reflecting plane; in this case the two are the same. Snell's law shows us that for a reflecting plane $\theta_i = \theta_r$ and, $\theta_t = \sin^{-1}\left(\sqrt{\frac{\varepsilon_1}{\varepsilon_2}}\sin(\theta_i)\right)$. Electric field equations are split into components that are normal and parallel to the plane of incidence, as follows:

i = incident wave: $$E_i = E_{ni}\cdot\hat{u}_n + E_{pi}\cdot\hat{u}_p \tag{5.5}$$

r = reflected wave: $$E_r = E_{nr}\cdot\hat{u}_n + E_{pr}\cdot\hat{u}_p \tag{5.6}$$

where p = parallel, n = normal and $\hat{u}_l$ is a unit vector in the l th direction.

Since this thesis uses a circularly polarized wave separated into its vector components, as will be discussed later, finding co- and cross- polarization reflection coefficients is not necessary. It is sufficient to find parallel and normal reflection coefficients, Γ_p and Γ_n from the following:

$$\Gamma_p = \frac{\eta_2\cos\theta_t - \eta_1\cos\theta_i}{\eta_2\cos\theta_t - \eta_1\cos\theta_i} \tag{5.7}$$

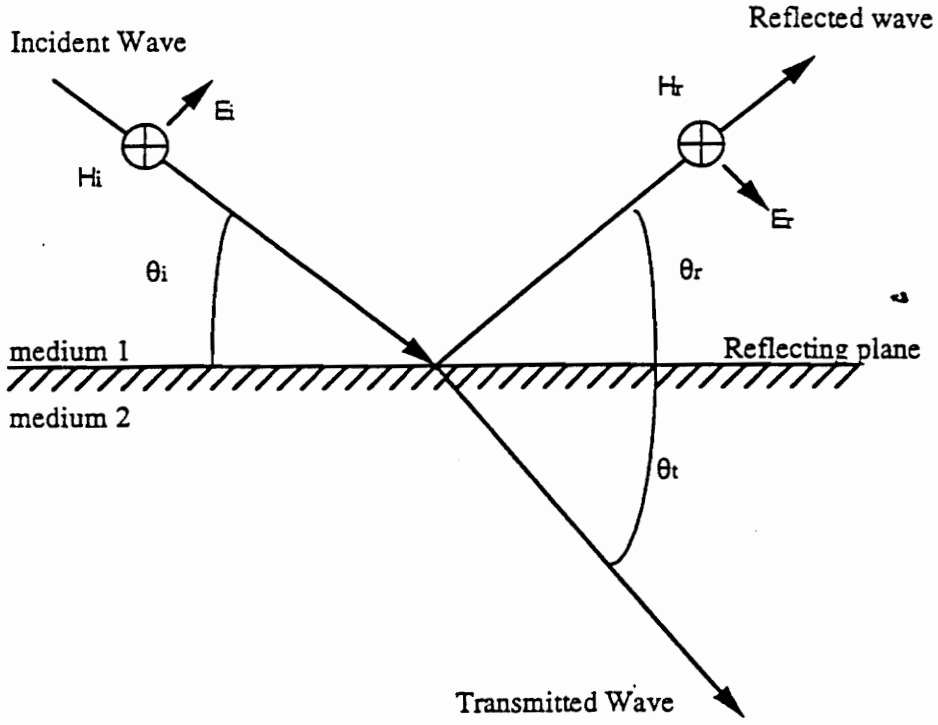

Figure 5.3.2 Reflection from a plane imperfect conductor with an obliquely incident linearly polarized wave.

$$\Gamma_n = \frac{\eta_2 \cos\theta_i - \eta_1 \cos\theta_t}{\eta_2 \cos\theta_i - \eta_1 \cos\theta_t} \tag{5.8}$$

i = incident and t = transmitted.

Where the intrinsic impedance is: $\eta_m = \sqrt{\frac{j\omega\mu_m}{\sigma_m + j\omega\varepsilon_m}} \quad [\Omega]$ (5.9)

and σ_m is the conductivity $(A/V \cdot m)$ of medium m, where $m \in [1,2]$.

For a perfect conductor, $\sigma_2 = \infty$ which makes $\eta_2 = 0$, therefore $\Gamma_p = \Gamma_n = -1$ which means that the sense of the polarization has switched. For an imperfect conductor, when an incoming wave is completely polarized in one sense, the reflected (scattered) wave will contain both senses. For the purposes of this thesis, the reflection coefficients, both normal and parallel, of a concrete surface must be calculated according to the procedure outlined above, for a number of different incidence angles. The results of this can be seen in Figures 5.3.3 and 5.3.4 magnitude and phase responses, respectively.

Each path's incoming circularly polarized electric field is decomposed into its vector components according to Equation 5.1 with the z-axis lying along the direction of propagation. Reflected rays are then put into the coordinate system of the line of sight ray and summed at the receiver.

Imitating Vogel's measurements, we find the calculated signal levels as the frequency is changed from 700 MHz to 1.8 GHz, while the receiver position, and the transmitting antenna elevation angle remain constant. To keep track of the phase and account for the field pattern of the receiving antenna, we must incorporate the vector effective length. The vector effective length incorporates the polarization state, the phase of the incoming electromagnetic wave and the effective aperture of the receiving antenna. To compare the signal levels predicted by this computer generated model, the antenna's open circuit voltage, V_{oc}, must be computed as:

$$V_{oc} = \hat{E} \bullet \vec{h} \qquad [V] \tag{5.10}$$

Here $\vec{h}$ is the vector effective length generalized to include the radiation pattern and polarization that is calculated, from Stutzman [STU93], by the relationship:

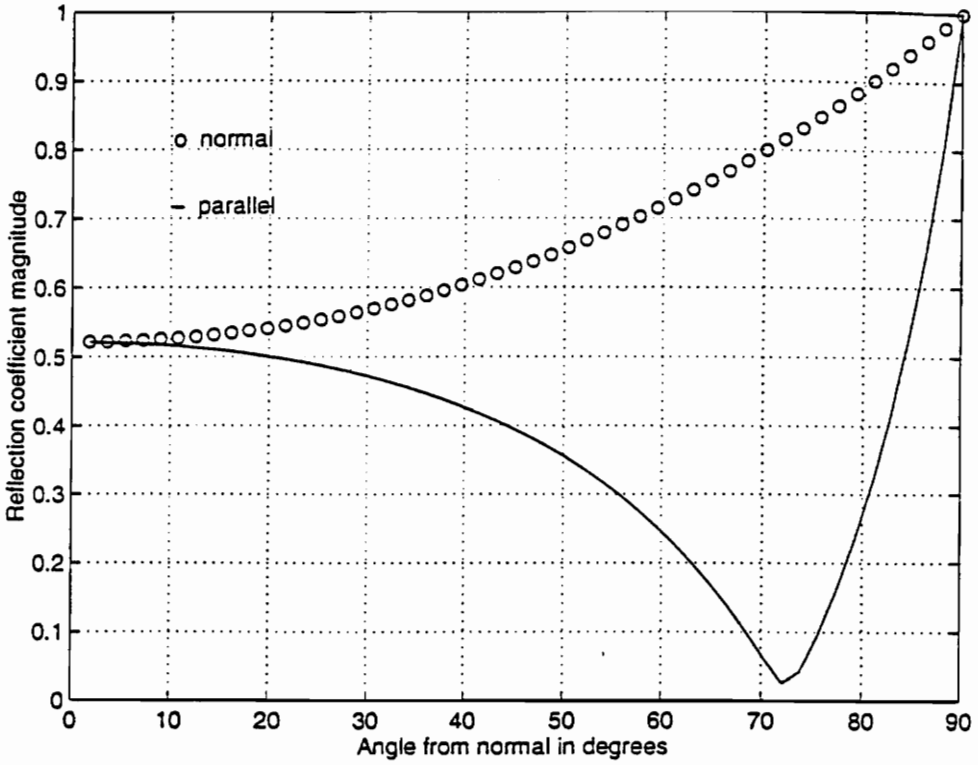

Figure 5.3.3 Reflection coefficient magnitude vs. incidence angle for concrete. (Complex relative permittivity = 10-j).

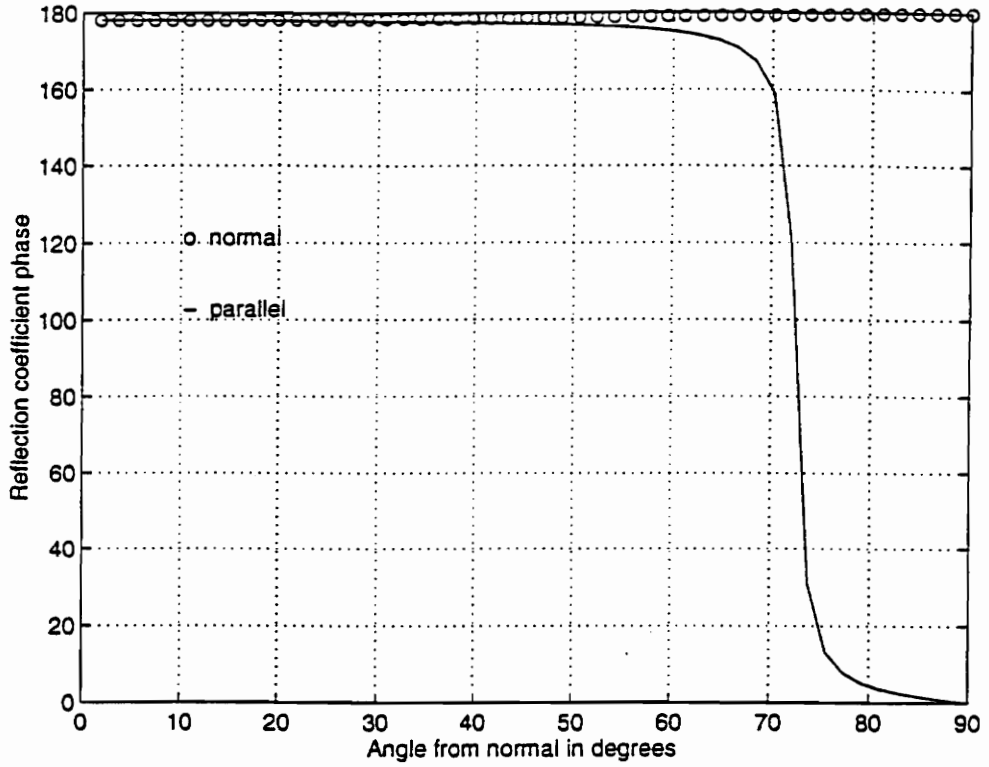

Figure 5.3.4 Reflection coefficient phase vs. incidence angle for concrete. (Complex relative permittivity = 10-j.)

$$\vec{h}(\theta,\phi) = 2\sqrt{A_e \frac{R_a}{\eta}} F(\theta,\phi)\hat{h} \quad [\text{m}] \qquad (5.11)$$

Where the vector effective length for a circularly polarized antenna is:

$$\hat{h} = \frac{\hat{x} + j\hat{y}}{2} \quad [\text{m}] \qquad (5.12)$$

and the intrinsic impedance of the medium, $\eta = \sqrt{\frac{\mu}{\varepsilon}}$ $[\Omega]$.

(5.13)

R_a is an assumed matched load resistance to the receiving antenna, A_e is the effective aperture of the receiving antenna, and $F(\theta,\phi)$ is the radiation field pattern of the receiving antenna. For a cavity backed spiral antenna such as the one Vogel used, the radiation field pattern is:

$$F(\theta,\phi) = \cos\left(0.53\theta^{5.8}\right) \qquad (5.14)$$

Vogel measured signal levels with respect to free space. To find the free space signal level V_{oc} was calculated for a single line-of-sight ray as in Section 5.1. This will be called $V_{oc_{fs}}$. To find the predicted value including reflections, V_{oc} including each reflected ray is calculated. This is called $V_{oc_{ref}}$. To account for the loss due to coupling, 5.5 dB, from [HOR86], was subtracted. Therefore the normalized signal level with respect to free space is:

$$V_{oc_n} = 20\log_{10}\left|\frac{V_{oc_{ref}}}{V_{oc_{fs}}}\right| - 5.5 \quad [\text{dB}] \qquad (5.15)$$

Using this background, a vector addition model can be created as follows:

1) Calculate the reflection coefficient from Equations 5.7 through 5.9 for a given angle of incidence and building construction (for concrete the relative permittivity was 10 - j).

2) Calculate the path length differences from Equation 5.4 with the given height of the receiver and elevation angle.

3) Decompose each ray into it's E-field components as in Equation 5.1, then multiply by the reflection coefficient calculated in step 1, for each reflection.

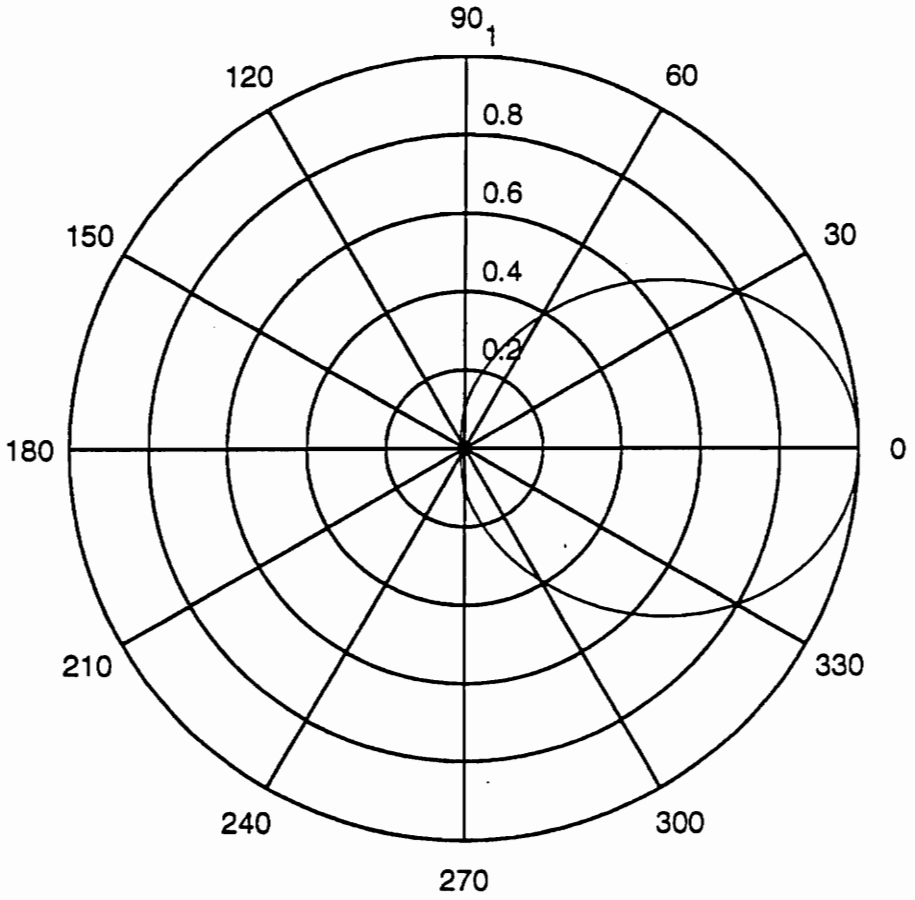

Figure 5.3.5 Field pattern for a cavity backed spiral antenna (see equation 5.14)

4) Put each reflected field into the same coordinate system as that of the LOS path, and multiply by the factor in Equation 5.14, where the antenna's boresight is pointed at the satellite (LOS path). Then add like components to yield the total E-field present at the receiver.

5) To find the open circuit voltage, find the dot product of the total E-field and the antenna's vector effective length given in Equation 5.10 where the part under the square root sign can be normalized to 1.

6) The signal is then normalized according to Equation 5.15.

7) To do a frequency sweep, as in Figure 5.3.6, steps 3 through 5 will have to be repeated for every frequency increment.

Figures 5.3.6 and 5.3.7 are the results of height and angle scans respectively, where the height of the receiver was varied while the angle was kept constant and vice versa. A search was conducted visually to find a good match for Vogel's results. Comparisons to the measured results obtained by Vogel are shown in Table 5.3.1. Here the model nulls and peaks are compared side by side with the measured nulls and peaks for the two ray model with a height of 1.5 meters and an elevation angle of 18 degrees. It is sufficient here to only examine the structure of the waveform.

Table 5.3.1 Comparison of two ray model and Vogel's figure 4 (measurements for BRC 15-24).

Model		Vogel		Model		Vogel	
Null freq.	Null level	Null freq.	Null level	Peak freq.	Peak level	Peak freq.	Peak level
		840 MHz	-30 dB			700 MHz	-1 dB
880 MHz	-10 dB					1020 MHz	-1 dB
		1100 MHz	-18 dB			1340 MHz	0 dB
		1500 MHz	-8 dB	1390 MHz	-2.5 dB		
		1710 MHz	-11 dB			1620 MHz	-2 dB
				Nulls		Peaks	
				Model	Vogel	Model	Vogel
Average	distance	between	nodes	0	290	0	306

As shown in the table, with only one null and one peak, it is clearly evident that the two ray model is not well suited to predict the signal levels measured by Vogel. A more precise model will have to be used, the next step is to try a three ray model presented in the next chapter.

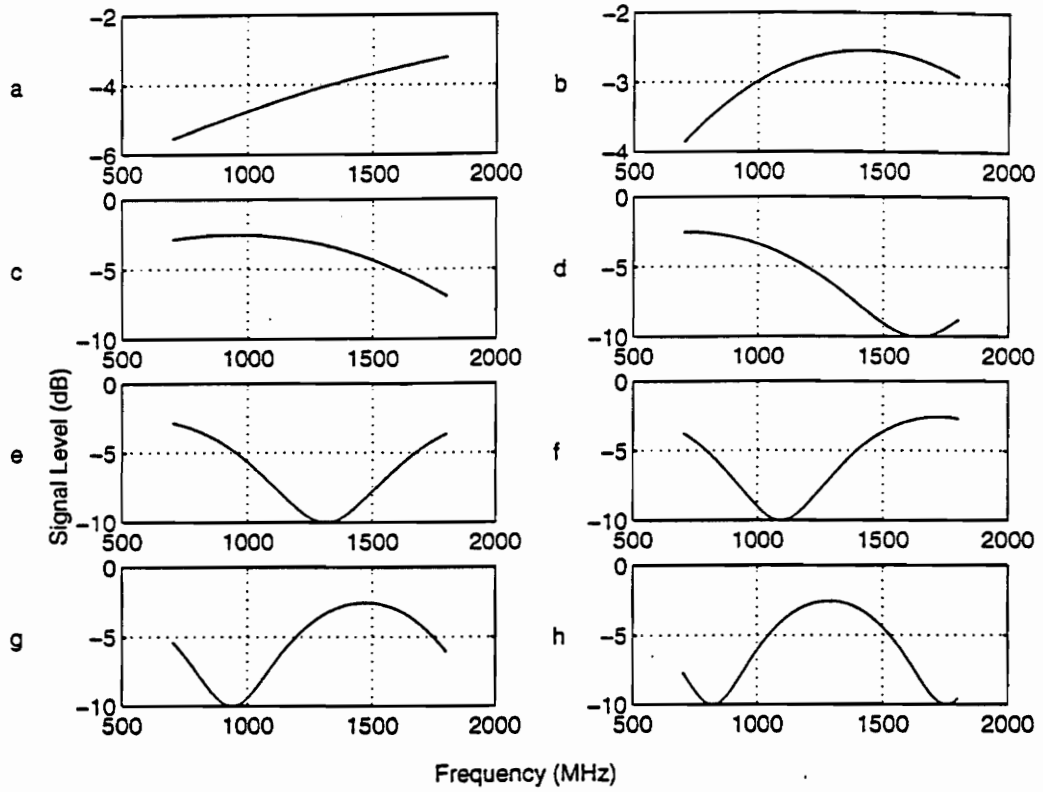

Figure 5.3.6 Signal level (dB) vs. frequency (MHz) for model 2. Height scan: height = .2 (a) to 1.6 (h) meters increasing in increments of .2 meters, angle = 18 degrees.

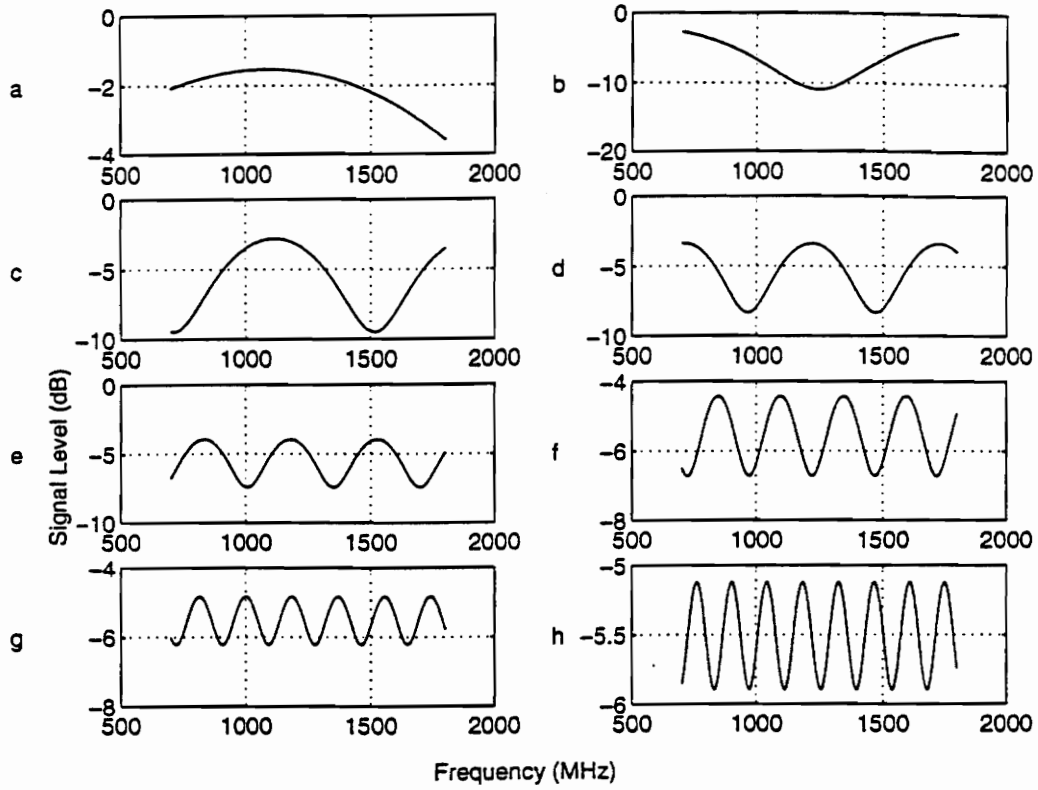

Figure 5.3.7 Signal level (dB) vs. frequency (MHz) for model 2. Angle scan: angle = 10 (a) to 45 (h) degrees increasing in increments of 5 degrees, height = 1.5 meters.

CHAPTER 6. THREE RAY MODEL (MODEL 3)

6.1 Introduction

A three ray model is assumed to have a satellite in orbit somewhere above a receiver located between two parallel plates, one represents the floor and one represents the roof or ceiling of a building. The distance to the satellite is great enough such that rays that are relatively close at the receiver location can be considered as being parallel to each other. This model examines the interaction among three rays of circularly polarized electromagnetic waves. Two rays are reflected, one off the floor, and one off the floor and the ceiling, these are combined with the line of sight ray at the receiver (see Figure 6.1.1).

The path length of ray 2 is greater than that of ray 1. The path length of ray 3 is greater than that of ray 2. The increase in path length is calculated in the following manner: according to Figure 6.1.1, an equiphase wavefront is drawn arbitrarily. For simplicity, it intersects the first point of reflection for each of the reflected rays. The satellite elevation angle is θ in our picture. To find the difference in path length between the LOS path and each reflected path, we must find the difference in length of each path after the equiphase wavefront.

For path 2:

$$p_2 = \frac{h}{\sin(\theta)} \quad [\text{m}] \tag{6.1}$$

$$p_1 = p_2 \cos(2\theta) \quad [\text{m}] \tag{6.2}$$

$$\text{difference} = p_2 - p_1 \quad [\text{m}] \tag{6.3}$$

where p_1 and p_2 are as defined earlier and in Figure 5.3.1.

For path 3:

$$f = \frac{b-h}{\sin(\theta)} \quad [\text{m}] \tag{6.4}$$

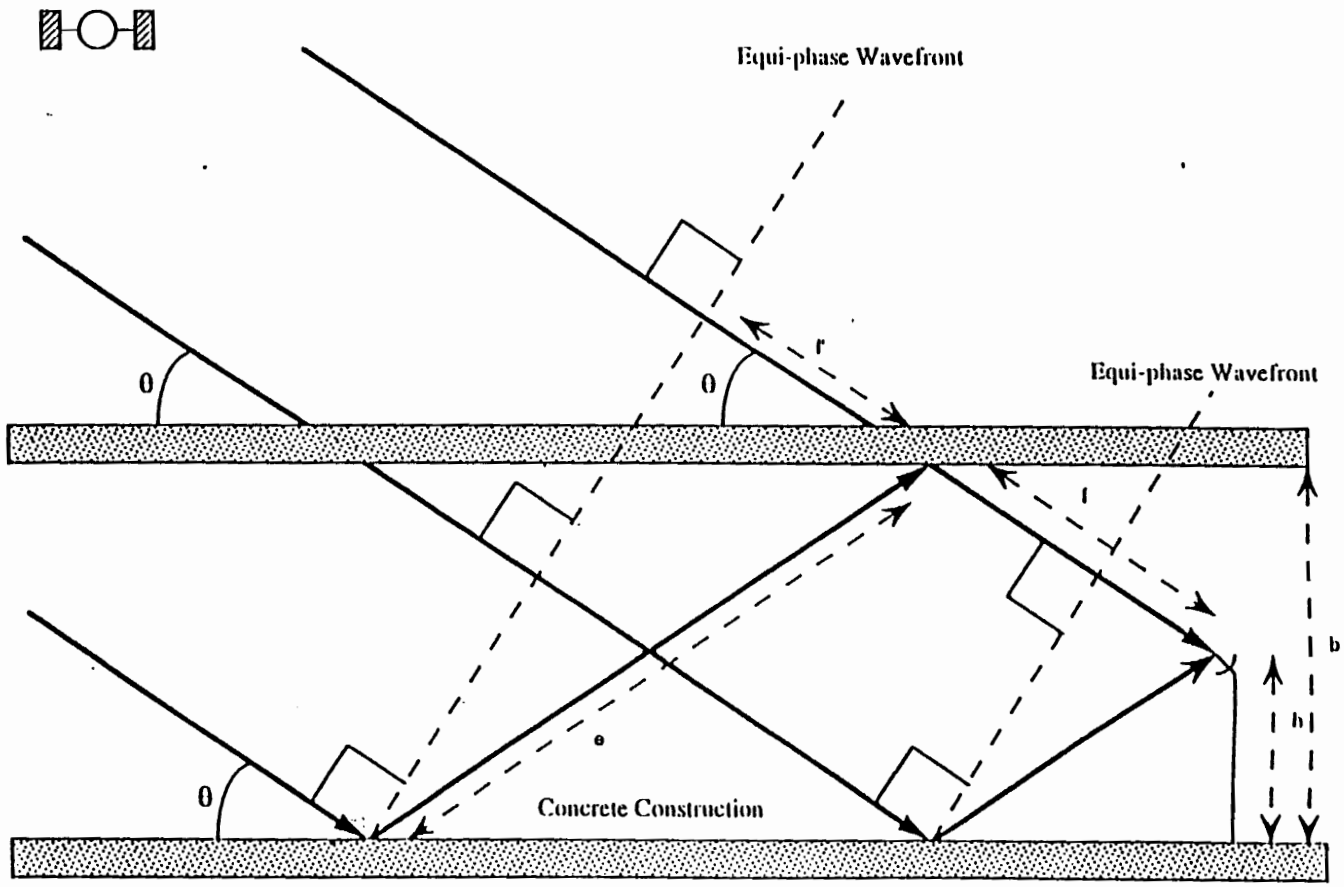

Figure 6.1.1 Three ray model. One line-of-sight ray and two reflected rays (Model 3).

$$e = \frac{b}{\sin(\theta)} \quad [\text{m}] \tag{6.5}$$

$$\begin{aligned} f' &= e\sin(90^\circ - 2\theta) \\ p_1' &= f + f' \\ p_3 &= e + f \\ diff &= p_3 - p_1' = e - f' \end{aligned} \quad [\text{m}] \tag{6.6}$$

where b, h, e, f, f', and θ are as shown in Figure 6.1.1.

Implementing the algorithm outlined in Chapter 5, only using the path length differences calculated in Equations 6.1 through 6.6, yields waveforms that can be seen to have similar properties as those of the figures in Vogel [VOG93] (see Figures 2.1.1 and 2.1.2). In addition, if the height of the receiving antenna and the elevation angle are made similar to those in Vogel, the resulting waveforms show the characteristic nulls at certain frequencies that were found in experimental results.

Comparisons to the measured results obtained by Vogel indicate that this may be a suitable model for the case of electromagnetic waves propagating from a satellite to a receiver inside a building.

6.2 Comparison to Vogel et al. for Building BRC-15-24

The measured electric field characteristics we are attempting to match are those of Figure 2.1.1 and Figure 2.1.2. Specifically in Figure 2.1.1 we want to reproduce the positions of the deep fade troughs that are present near 800 and 1100 MHz, and again at 1700 MHz., and the approximate distance between each null and each peak that occur with what appear to be a constant period. The receiver height, h, is approximately 1.4 meters, and the elevation angle, θ , of the mock satellite setup is approximately 18 degrees. Therefore, a search at a range of heights centered at 1.4 meters with the elevation angle set at approximately 18 degrees was performed to find a waveform that matches. Figure 6.2.1 is a composite of eight different receiver heights where the elevation angle is kept constant at 19 degrees and the frequency is again swept from 700 MHz to 1800 MHz. It can be seen that there are present the deep fade troughs apparent

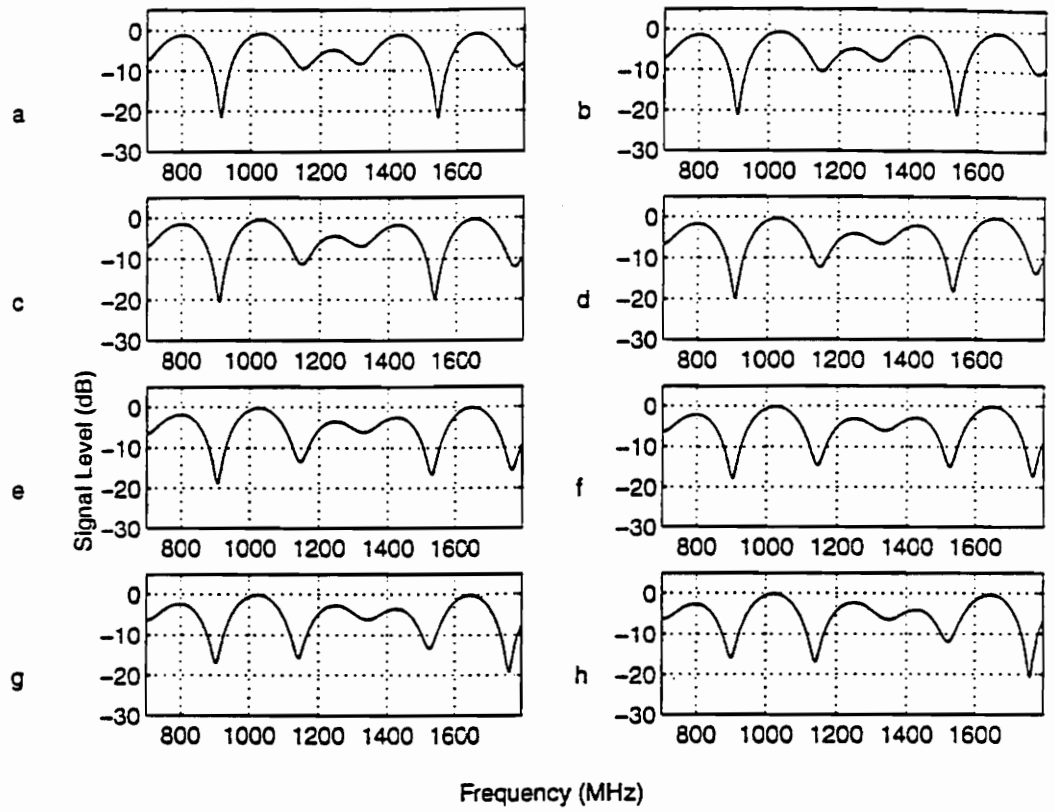

Figure 6.2.1 Signal level (dB) vs. frequency (MHz) for model 3. Height scan: height 1.46 (a) to 1.53 (h) meters increasing in increments of .01 meters, angle = 19 degrees.

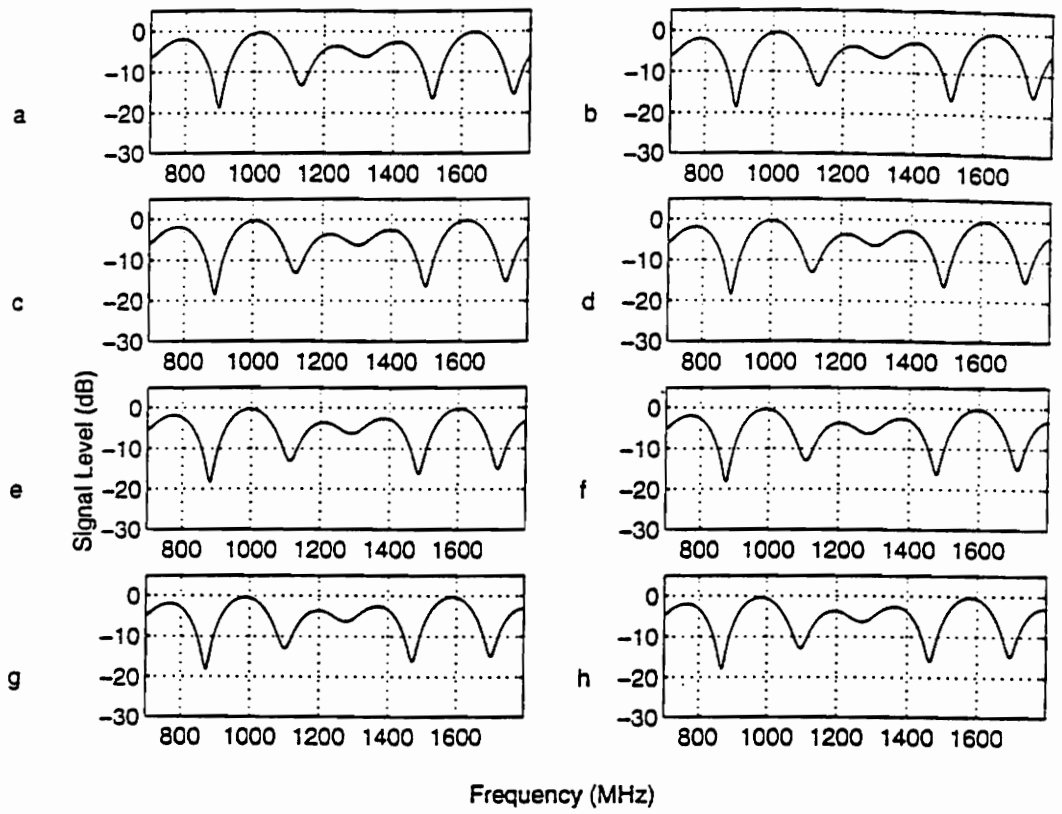

Figure 6.2.2 Signal level (dB) vs. frequency (MHz) for model 3. Angle scan: angle = 19.2 (a) to 19.9 (h) degrees increasing in increments of .1 degrees, height = 1.5 meters.

in Vogel [VOG93]. Here graphs (a) through (h) vary in height from 1.46 to 1.53 meters in increments of .01 m. An angle scan was then performed at a height of 1.5 meters with a range of elevation angles centered at 19.5 degrees (see Figure 6.2.2). As the height is changed the node that receives the greatest fading changes, and as the elevation angle is changed, the distance between the nodes is changed in a straight forward manner. From this we can see that one possible choice for a match is with h = 1.5 m and θ = 19.6 degrees, here there are nulls that appear at approximately 880 MHz, 1110 MHz, 1290 MHz, 1480 MHz and also at 1720 MHz, which can also be seen in Vogel's results, summarized in Table 6.2.1. A close-up of this result is seen in Figure 6.2.3, the nodes are roughly the same distance apart as those in Vogel. Here again as in Chapter 5 the model nulls and peaks are compared to the measured nulls and peaks in Table 6.2.1. This fit to Vogel's measurements is done visually, comparing the frequency positions of the nulls.

Table 6.2.1 Comparison of Figure 6.2.4 (three ray model) and Vogel's Figure 4 (measurements for BRC 15-24).

Model 3		Vogel		Model 3		Vogel	
Null freq.	Null level	Null freq.	Null level	Peak freq.	Peak level	Peak freq.	Peak level
		840 MHz	-30 dB			700 MHz	-1 dB
880 MHz	-19 dB			770 MHz	-3 dB		
1110 MHz	-13 dB	1100 MHz	-18 dB	990 MHz	-2 dB	1020 MHz	-1 dB
1290 MHz	-7 dB			1200 MHz	-4 dB		
1480 MHz	-17 dB	1500 MHz	-8 dB	1380 MHz	-3 dB	1340 MHz	0 dB
1720 MHz	-16 dB	1710 MHz	-11 dB	1600 MHz	-1 dB	1620 MHz	-2 dB
				1800 MHz	-3 dB		
				Nulls		Peaks	
				Model 3	Vogel	Model 3	Vogel
Average	distance	between	nodes	210	290	206	306

Vogel then increased the height of the receiver and took measurements over a range of frequencies as before. This provides a good test of the accuracy of our model. Several things must now be taken into account before we proceed. A change in the height of the receiver will produce a change (however small) in the elevation angle of the satellite

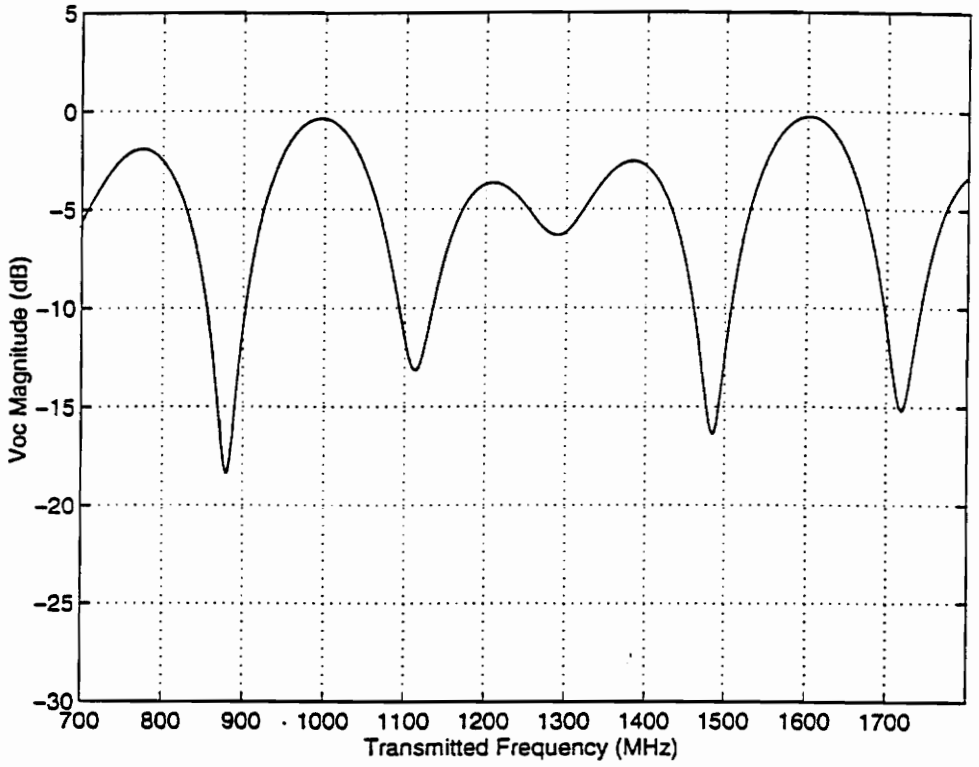

Figure 6.2.3 Signal level (dB) vs. frequency (MHz) for model 3. where angle = 19.6 degrees, and height = 1.5 meters.

as seen by the receiver. If this simulation were done with a real satellite transmission, the change in height would have produced a negligible change in the elevation angle. However Vogel used a transmitter mounted upon a tower to simulate the path of the satellite transmission. The van is located a finite (and relatively small) distance from the receiver, a change in the height of the receiver may produce a significant change in the elevation angle:

$$\begin{aligned} h &= 52\tan(\theta) \\ \theta &= \tan^{-1}\left(\frac{h-5}{52}\right) \end{aligned} \tag{6.7}$$

The elevation angle can decrease as much as one degree for a reasonably small increase in receiver height. A scan of height was then done centered at 2.0 meters (previous + .5 meters) and at an angle of 19 degrees. An angle scan was then performed centered at 19 degrees to account for the supposed decrease in elevation angle. A clear match to the measured results can be seen in Figure 6.2.4, with a height of 2.04 meters and an angle θ = 19 degrees. Nulls occur approximately at 900, 1110, 1340 and 1550 MHz as well as at 1770 MHz corresponding to Figure 2.1.2 results are summarized in Table 6.2.2. Measurements of the distance between consecutive nulls and consecutive peaks show that the distance is fairly constant.

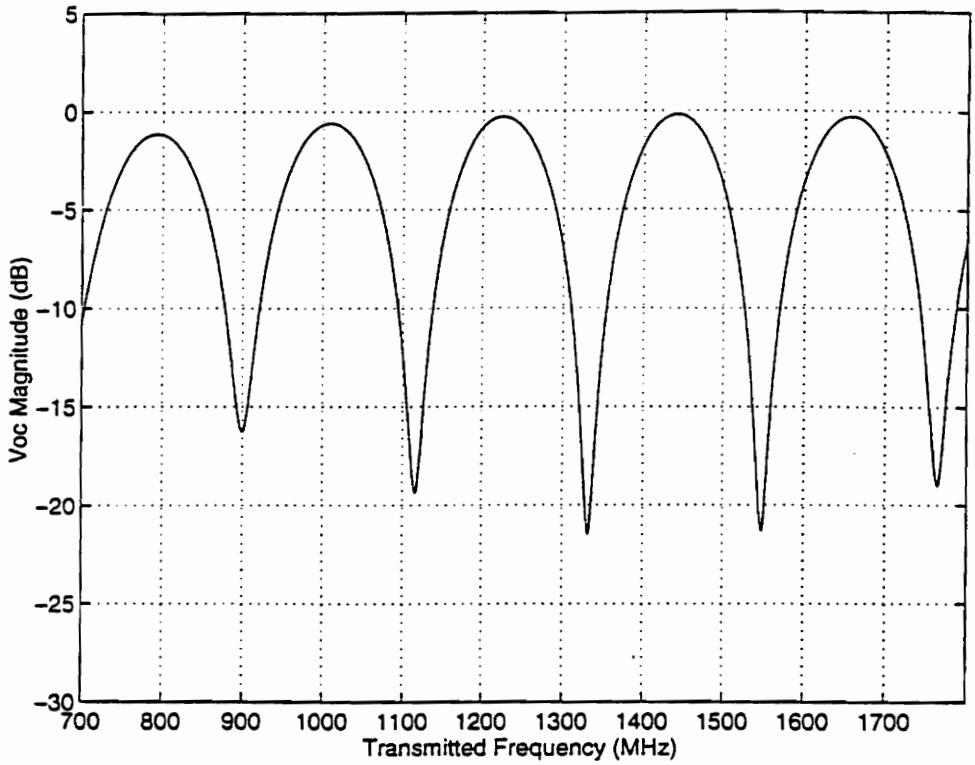

Figure 6.2.4 Signal level (dB) vs. frequency (MHz) for model with angle = 19 degrees, and height = 2.04 meters.

Table 6.2.2 Comparison of Figure 6.2.6 (three ray model) and Vogel's Figure 5 (measurements for BRC 15-24).

Model 3		Vogel		Model 3		Vogel	
Null freq.	Null level	Null freq.	Null level	Peak freq.	Peak level	Peak freq.	Peak level
		720 MHz	-12 dB	800 MHz	-2 dB	770 MHz	-5 dB
900 MHz	-17 dB	900 MHz	-14 dB	1010 MHz	-2 dB	1000 MHz	-2 dB
1110 MHz	-20 dB	1050 MHz	-8 dB			1120 MHz	-2 dB
		1200 MHz	-7 dB	1230 MHz	-1 dB	1290 MHz	-1 dB
1340 MHz	-22 dB	1370 MHz	-24 dB	1440 MHz	-1 dB	1440 MHz	-7 dB
1550 MHz	-22 dB	1520 MHz	-30 dB			1610 MHz	-5 dB
		1660 MHz	-12 dB	1660 MHz	-1 dB		
1770 MHz	-19 dB	1780 MHz	-16 dB			1710 MHz	-3 dB
				Nulls		Peaks	
				Model 3	Vogel	Model 3	Vogel
Average	distance	between	nodes	220	154	215	156

6.3 Comparison to Vogel et al. for Commons

The building labeled Commons is a structure in which a large portion of one wall is a window. The overall construction is similar to that of BRC-15-24 i.e. a concrete construction and the mock satellite setup is set at an angle of 16 degrees. Vogel's measurements are shown in Figure 2.1.3. There are the same characteristic deep fades as reported earlier for BRC 15-24, and the distance between consecutive nulls or consecutive peaks is relatively constant as shown earlier. Using this simulation at an elevation angle of 16 degrees, a height scan is performed. The height is determined to be approximately 1.3 meters. An angle scan was then performed. This revealed that 16.0 degrees was the best match. Figure 6.3.1 shows the best fit for Figure 2.1.3. Here again the constancy between consecutive nulls or peaks can be seen.

Table 6.3.1 Comparison of Figure 6.3.2 (three ray model) and Vogel's Figure 9 (measurements for Commons).

Model 3		Vogel		Model 3		Vogel	
Null freq.	Null level	Null freq.	Null level	Peak freq.	Peak level	Peak freq.	Peak level
820 MHz	-22 dB	900 MHz	-30 dB	700 MHz	-4 dB	700 MHz	-9 dB
				980 MHz	-1 dB		
1110 MHz	-11 dB			1200 MHz	-6 dB	1150 MHz	-10 dB
1300 MHz	-10 dB	1250 MHz	-24 dB	1450 MHz	-1 dB	1400 MHz	-9 dB
1590 MHz	-23 dB	1650 MHz	-30 dB	1710 MHz	-3 dB	1750 MHz	-15 dB
				Nulls		Peaks	
				Model 3	Vogel	Model 3	Vogel
Average	distance	between	nodes	257	375	253	350

The receiver is then moved to a position behind a window where the attenuation due to the wall is not the same for every ray. The LOS path clearly dominates. The deep fade troughs that are present in the other measurements are not present here. Differences between peak and null are less than 6 dB. To simulate this, the ray that simulates the LOS path is multiplied by $\frac{1}{T}$ where T is the transmission coefficient of concrete, from [HOR86] $T = 10^{-5.5/20} = .5309$. Figure 6.3.2 is a simulation with the height at 1.3 meters and the elevation angle at 16 degrees, the difference between peak and null is less than 3 dB. This is a match for Figure 2.1.4 results are summarized in Table 6.3.2.

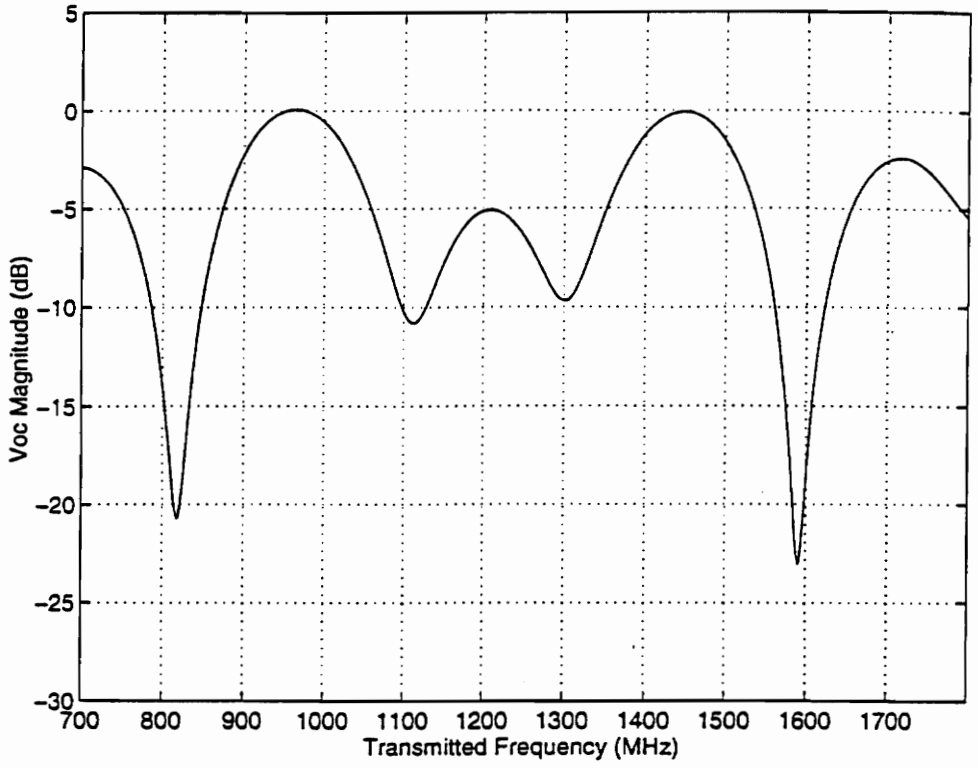

Figure 6.3.1 Signal level (dB) vs. frequency (MHz) for model 3 with angle = 16 degrees, and height = 1.3 meters.

Table 6.3.2 Comparison of Figure 6.3.4 (three ray model) and Vogel's Figure 10 (measurements for Commons).

Model 3		Vogel		Model 3		Vogel	
Null freq.	Null level	Null freq.	Null level	Peak freq.	Peak level	Peak freq.	Peak level
830 MHz	-5 dB			700 MHz	1.5 dB		
		940 MHz	-7 dB			810 MHz	-2 dB
1100 MHz	-2.5 dB			970 MHz	3.5 dB		
		1250 MHz	-2 dB	1210 MHz	0 dB	1160 MHz	1 dB
1310 MHz	-2.5 dB			1450 MHz	3.5 dB	1440 MHz	4 dB
1600 MHz	-6 dB	1600 MHz	-2 dB	1720 MHz	2 dB	1710 MHz	2 dB
				Nulls		Peaks	
				Model 3	Vogel	Model 3	Vogel
Average	distance	between	nodes	256	330	253	300

For typical use where the receiver is at a height between 1.5 and 2 meters and the LOS path is obstructed along with the two other paths, and the elevation angle is 19.6 degrees, the signal statistics look as shown in Table 6.3.3. Here signal levels were found for a particular frequency at several different values of receiver height, between 1.5 and 2 meters. Statistics such as minimum, maximum, mean and standard deviation all measured in dB below free space, were compiled for each frequency band. Where 880 MHz corresponds to a null at 1.5 m, 920 MHz corresponds to a mid-range value of a null, and 990 MHz is a peak at 1.5 m.

Table 6.3.3 Model 3 statistics for typical use.

	Minimum	Maximum	Mean	Std. Dev.
880 MHz	-19.18 dB	-10.07 dB	-5.87 dB	4.12 dB
920 MHz	-12.58 dB	-7.17 dB	-3.95 dB	2.87 dB
990 MHz	-4.87 dB	-.26 dB	-2.07 dB	1.63 dB

These results are significant in that they show that the user has to move less than a half meter to find a spot where reception is good. A change in receiver height of only 50 cm can reduce fading bringing signal levels better than -10 dB.

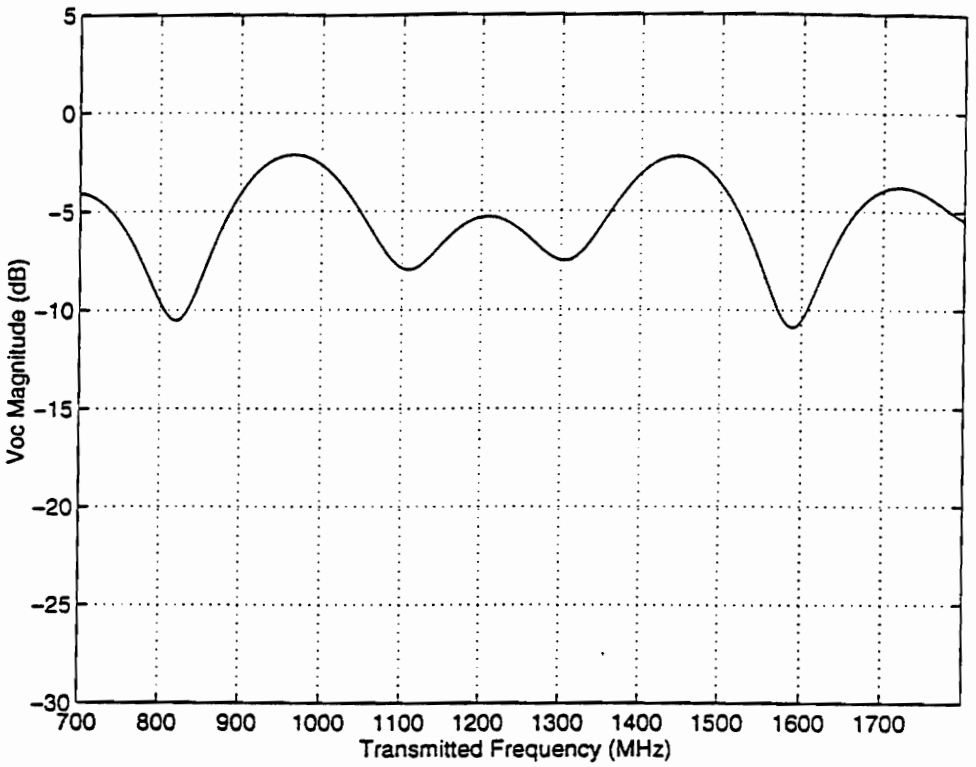

Figure 6.3.2 Signal level (dB) vs. frequency (MHz) for model 3 with angle = 16 degrees, and height = 1.3 meters. Line-of-sight path is through a window.

Figure 6.3.2 Signal level (dB) vs. frequency (MHz) for model 3 with angle = 16 degrees, and height = 1.3 meters. Line-of-sight path is through a window.

6.4 Power Delay Profile

Seidel [SEI92] defines two measures of delay spread, primarily, mean excess delay spread and RMS delay spread.

6.4.1 Mean Excess Delay Spread

Mean Excess Delay Spread is defined as the first moment of the power delay profile:

$$\bar{\tau} = \frac{\sum_k \alpha_k^2 \tau_k}{G_r} \tag{6.8}$$

where $G_r = \sum_k \alpha_k^2$ (6.9)

and α_k = Power of the k^{th} multipath component.

τ_k = Time delay of the k^{th} multipath component.

6.4.2 RMS Delay Spread

RMS Delay Spread is defined as the square root of the second central moment of the power delay profile:

$$\sigma_\tau = \sqrt{\overline{\tau^2} - \bar{\tau}^2} \tag{6.10}$$

where $\overline{\tau^2} = \frac{\sum_k \alpha_k^2 \tau_k^2}{G_r}$. (6.11)

Above are the typical methods of representing the power delay profile. Vogel however finds the percentage of the total power received as a function of time. The models presented here give the electric fields seen at the receiver from the various multipath components. To duplicate what Vogel has done, the power garnered from each

path's electric field components must be calculated. Beckmann defines flux density in terms of the electric field as: $S = \frac{1}{2\eta}\left(E_x^2 + E_y^2\right)$ [W/m^2] (6.12)

This is the standard Poynting vector.

The power received in watts from the antenna is

$$P = SA_e \quad [W] \tag{6.13}$$

where A_e is the effective aperture of the antenna

$$A_e = A_e\left|F(\theta,\phi)\right|^2 \tag{6.14}$$

this is direction dependent where $F(\theta,\phi)$ is the antenna's field pattern (see Equation 5.14). This definition for the power is convenient for this work since the basis for the models here is the decomposition of the electric field into its x and y components. Therefore power calculations are simple.

Figure 6.4.1 is a representation of the power delay profile for model 3 with h = 1.5 meters. Here the power is given as a percentage of the total power after a certain time. Since only three rays are accounted for, there are only three points before 100 % of the arriving power has arrived. Figure 2.1.5 shows the cpf of three of the six buildings studied in Vogel [VOG93]. After approximately 6 ns 85% of the power arriving has arrived at the receiver and after 50 ns, 99% of the power has arrived (for BRC 15-24). However this is taking into account possibly on the order of 100 different paths. Figure 6.4.1 shows that for this simulation 85% of the power arrives after approximately 3 ns and 100 % of the power arrives 4.5 ns after the first signal arrives while only taking into account three paths. After about 80 ns in Vogel's measurements, 100 % of the total power has arrived. Most of the arriving power in Figure 2.1.5 is at the receiver by 6 ns, so if Vogel's power delay profile were to include only the most significant paths, the agreement with the model presented here would be much greater.

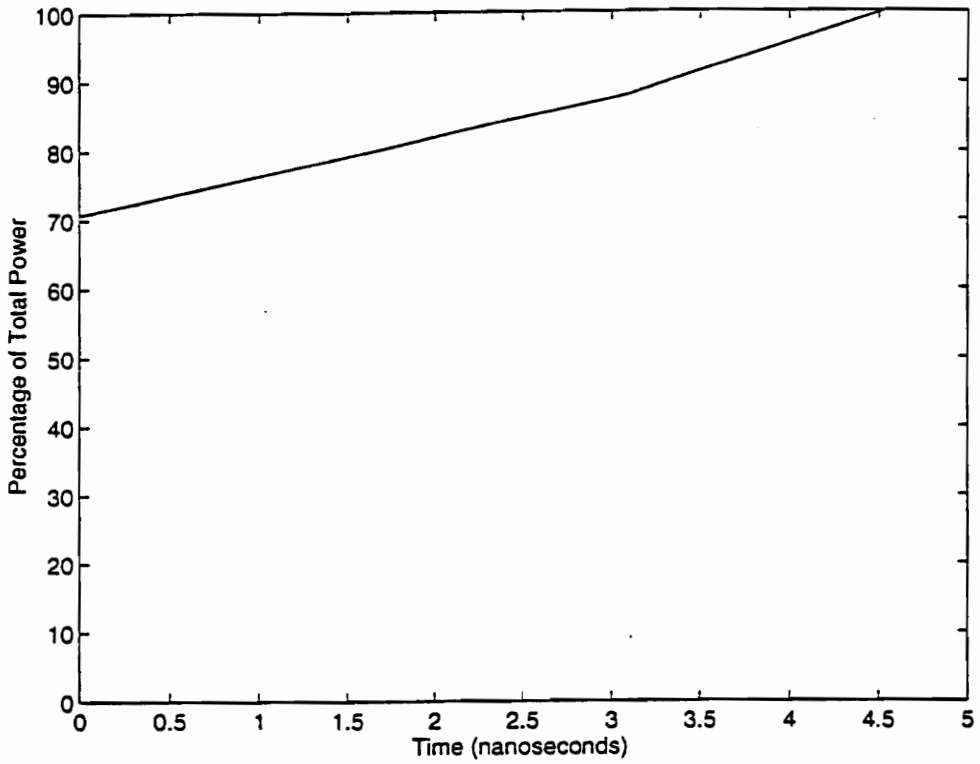

Figure 6.4.1 Power delay profile. Percentage of total power (%) vs. time (ns) for model 3 with height = 1.5 meters, and angle = 19.6 degrees.

Chapter 7. Conclusion

This thesis provides an analysis of several models for the prediction of satellite signal levels inside buildings, including statistical models, cavity mode models and multipath models. From the work presented in this thesis, one is able to make the following conclusions:

1) A three ray model, incorporating LOS, floor, and ceiling reflected rays gives reasonable agreement with Vogel's data. The types of information needed are the room height, the receiver height, if the receiver is in the vicinity of a window, and the elevation angle of the satellite.

2) The cavity mode approach doesn't work because of the uniqueness problem outlined in Chapter 4, too many potential modes and no obvious way to decide between them.

3) This model shows that a user has to move only a small distance to find an area where fading is minimized

This model might be of help to designers of satellite systems in that they would be able to predict what the magnitude of losses might be and could then design a system to operate despite such conditions.

Future Work

In the future it may be possible to solve the cavity resonator problem and possibly produce a better model, if a way of determining the modes that are excited can be found. To create a more accurate model the interactions with other types of objects in the room may have to be examined or accounted for, i.e. fluorescent lights, CRTs and possibly wireless LANs. Finally it may be worth the effort to determine if this model is useful for other building types and constructions.

References

[AMO93] F. Amoroso and W. W. Jones, "Geometric model for DSPN satellite reception in the dense scatterer mobile environment", IEEE Transactions on Communications, vol. 41, no. 3, March 1993, pp. 450- 454.

[BEC68] P. Beckmann, The Depolarization of Electromagnetic Waves, The Golem Press, Boulder, CO 1968.

[BOS86] C.W. Bostian, T. Pratt, Satellite Communications, John Wiley & Sons, New York, 1986, pp. 104 - 148.

[BUL87] R. Bultitude "Measurement, characterization and modeling of indoor 800/900 MHz radio channels for digital communications", IEEE Communications Magazine, vol. 25, no. 6, June 1987, pp. 5-12.

[BUL89] R. Bultitude, S. Mahmoud, and W. Sullivan, "A comparison of indoor radio propagation characteristics at 910 MHz and 1.75 GHz." IEEE Journal on Selected Areas in Communications, vol. 7, no. 1, January 1989, pp.20-30.

[COX83] Cox, D.C., Murray, R.R., and Norris, A.W., "Measurements of 800 MHz radio transmissions into buildings with metallic walls", Bell System Technical Journal, vol. 62, no. 9, 1983, pp. 2695-2717.

[COL85] Collin, R.E., Antennas and Radiowave Propagation, McGraw-Hill Book Company, New York, 1985.

[COU93] L.W. Couch II, Digital and Analog Communication Systems, MacMillan, New York, 1993.

[DAN71] Cuthbert Daniel, Fred S. Wood, Fitting Equations to Data, Wiley-Interscience, New York, 1971.

[DEV87] D. Devasirvatham, "A comparison of time delay spread and signal level measurements within two dissimilar office buildings", IEEE Transactions on Antennas and Propagation, vol. AP-35, no. 3, March 1987,pp. 852-856.

[DEV87J] D. Devasirvatham, "Multipath time delay spread in the digital portable radio environment" IEEE Communications Magazine, vol. 25, no. 6, June 1987, pp.13-21.

[DEV89] D. Devasirvatham, "Time delay spread measurements at 850 MHz and 1.7 GHz inside a metropolitan office building." Electronics Letters, vol. 25, no. 3, 1989, pp. 950-951.

[EDN94] "Communicating by satellite", EDN August 18, 1994, volume 39, number 17, p. 58.

[FLO87] W.L. Flock, Propagation Effects on Satellite Systems Below 10 GHz, NASA Reference Publication 1108(02), December 1987.

[HOE92] P. Hoerher, "A statistical discrete-time model for the WSSUS multipath channel", IEEE Transactions on Vehicular Technology, vol. 41, no. 4, November 1992, pp 461-468.

[HON92] W. Honcharenko, H.L. Bertoni, J. Dailing, J. Qian, H.D. Yee, "Mechanisms governing UHF propagation on single floors in modern office buildings", IEEE Transactions on Vehicular Technology, vol. 41, no. 4, November 1992, pp. 496-504.

[HON93] W. Honcharenko, H.L. Bertoni, J. Dailing, "Mechanisms governing propagation between different floors in buildings", IEEE Transactions on Antennas and Propagation, vol. 41, no. 6, June 1993, pp.787-790.

[HOR86] J. Horikoshi, K. Tanaka, and T. Morinaga, "1.2 GHz band wave propagation measurements in concrete building for indoor radio communication", IEEE Transactions on Vehicular Technology, vol. VT-35, no. 4, November 1986, pp.146-152.

[HOW92] S.J. Howard, K. Pahlavan, "Auto-regressive modeling of wide band indoor radio propagation", IEEE Transactions on Communications, vol. 40, no. 9, September 1992, pp.1540-1552.

[HUI94] J. T. Huiid, J. B. Andersen, J. Toftgard, and J. Bojer "Terrain based propagation models of microwave signals scattered from buildings", IEEE Transactions on Antennas and Propagation, vol. 42, no. 8, August 1994, pp. 1126-1137.

[IPP86] L.J. Ippolito Jr., Radio Wave Propagation In Satellite Communications, Van Nostrand Reinhold Co., New York, NY. 1986.

[JOR68] E. C. Jordan, K.G. Balmain, Electromagnetic Waves and Radiating Systems, Prentice-Hall, Inc. Englewood Cliffs, NJ 1968.

[KAU95] U. Kauschke, "Propagation and system performance simulations for the short range DECT system in microcellular urban roads"; IEEE Transactions on Vehicular Technology, vol. 44, no. 2, May 1995, pp. 253-260.

[LAF90] J. F. Lafortune M. Lecours, "Measurement and modeling of propagation losses in a building at 900 MHz", IEEE Transactions on Vehicular Technology, vol. 39, no. 2, May 1990, pp. 101-108.

[LIA80] S.Y. Liao, Microwave Devices and Circuits, Prentice-Hall, Englewood Cliffs, NJ, 1980.

[LOT94] T. Lo, J. Litra, and H. Leung, "A new approach for estimating indoor radio propagation characteristics", IEEE Transactions on Antennas and Propagation, vol. 42, no. 10, October 1994, pp. 1369-1376.

[MOL91] D. Molkdar, "Review on radio propagation into and within buildings", IEE Proceedings-H, vol. 138, No. 1, February 1991, pp.61-73.

[RAP89] T. S. Rappaport, "UHF fading in factories.", IEEE Journal on Selected Areas in Communications, vol. 7, p. 40-48, January 1989, pp40-48.

[RAP89A] T. S. Rappaport, "Characterization of the UHF multipath radio channel in factory buildings.", IEEE Transactions on Antennas and Propagation, vol. 37, p.1058 - 1069, August 1989, pp.1015-1017.

[RAP94] T. S. Rappaport, Sandip Sandhu, "Radiowave propagation for emerging wireless personal communication systems", Proceedings of Virginia Tech's 4th Symposium on Wireless Personal Communications, June 1994, pp.1-27.

[REF69] Reference Data for Radio Engineers, Fifth Edition, H.W. Sams and Co. Inc., Indianapolis/ Kansas City/ New York, March 1969.

[SEI92] S. Y. Seidel and T. S. Rappaport, "914 MHz path loss prediction model for indoor wireless communications in multifloor buildings", IEEE Transactions on Antennas and Propagation, vol. 40, no. 2, February 1992, pp.207-217.

[SEI93] S.Y. Seidel, Site Specific Propagation Prediction for Wireless In-Building Personal Communication System Design, 1993.

[SHE93] A. U. Sheikh, M. Handforth, and M. Abdi, "Indoor mobile radio channel at 946 MHz: measurements and modeling", Carleton University Research Report, 1993, pp. 73-76.

[STU93] W.L. Stutzman, Polarization In Electromagnetic Systems, Artech House, Norwood, MA 1993.

[STU94] W.L. Stutzman, Personal communication, October, 1994.

[TAN95] S. Y, Tan, and H. S. Tan, "Propagation model for microcellular communications applied to path loss measurements in Ottawa city streets", IEEE Transactions on Vehicular Technology, vol. 44, no. 2, May 1995, pp. 313-317.

[TUR88] A.M.D. Turkmani, and J.D. Parsons, "Measurement of building penetration loss on radio signals at 441, 900, and 1400 MHz", Journal of IERE, vol. 58, no. 6, 1988, pp.169-174.

[VOG93] W.J. Vogel and G.W. Torrence, "Propagation measurements for satellite radio reception inside buildings", IEEE Transactions on Communications, vol. 41, no. 7, July 1993, pp. 954-961.

[VOG95] W.J. Vogel, H. Ling, and G.W. Torrence, "Fluorescent light interaction with personal communications signals", IEEE Transactions on Communications, vol. 43, no. 2,3,4, February / March / April 1995, pp. 194-197.

Appendix

MATLAB code:

```
% gamma.m
%
% calculates the reflection and transmission
% coeficient for a given angle and relative
% permittivity

% returns parallel and normal reflection
% and transmission coefficients


function [gp,gn,tp,tn] = gamma(el,ang);

% Constants

mu0 = pi*4e-7;          % Permeability of F.S.
mul = mu0;
e0 = 8.854e-12;         % Permittivity of F.S.
el = el*e0;

n0 = sqrt(mu0/e0);      % Intrinsic impedances
n1 = sqrt(mul/el);

angt = asin(sqrt(e0/el)*sin(ang));              % Transmission Angle
%ang,angt

% Parallel reflection coefficient
gp = (n1*cos(angt) - n0*cos(ang))/((n1*cos(angt) + n0*cos(ang)));

% Normal reflection coefficient
gn = (n1*cos(ang) - n0*cos(angt))/((n1*cos(ang) + n0*cos(angt)));

% Co-polarized reflection coefficient
gc = .5*(gn-gp);

% Cross-polarized reflection coefficient
gx = .5*(gn+gp);

% Parallel transmission coefficient
tp = 2*n1*cos(ang)/((n1*cos(angt) + n0*cos(ang)));

% Normal transmission coefficient
tn = 2*n1*cos(ang)/((n1*cos(ang) + n0*cos(angt)));

% Parallel reflection coefficient
gp1 = (n0*cos(ang) - n1*cos(angt))/((n0*cos(ang) + n1*cos(angt)));

% Normal reflection coefficient
gn1 = (n0*cos(angt) - n1*cos(ang))/((n0*cos(angt) + n1*cos(ang)));

tp = tp*gp1;
tn = tn*gn1;
```

```
% Model 2c
% Models a circularly polarized wave incident upon a receiver
%  and a single reflected path off the ground.
% Sattelite is said to be at infinity
% Antennae is at a fixed height and the
% Frequency is swept from 700MHz to 1.8GHz
% Reflection coefficients calculated using Gamma subroutine

% Eo amplitude of E-field
% This is circularly polarized so the amplitude of the vector is constant

Eo = 1;

% Constants

z = 0;                          % Arbitrary z value
c = 3e8;                        % Speed of light
e0 = 8.854e-12;                 % Permittivity of free space
mu0 = pi*4e-7;                  % Permeability of free space

ctr = 0;                                % counter
for f = 7e8:1e6:18e8;
        ctr = ctr + 1;          % Increment Counter
        fr(ctr) = f*1e-6;               % Operating Frequency
        w(ctr) = 2*pi*f;                % Frequency in Radians
        k(ctr) = w(ctr)*(sqrt(e0*mu0));% Phase constant
end

% Circularly polarized field equation
for i = 1:ctr
        x(i) = exp(j*k(i)*z);
        y(i) = exp(j*(k(i)*z + pi/2));
%       Ec(i) = Eo*(x(i)^2 + y(i)^2)^.5;
end


%for nt = 1:10
ang = 18; %
%ang = 5.0 + 5*nt               % Elevation angle of the satellite
ang = 90 - ang;                 % Converts elevation angle to incidence
rad = ang*pi/180;       % Converts angle to radians

% Calculation of reflection coefficient

e1 = 10-j;                      % Complex permittivity of concrete
[tau1,tau2,gc,gx] = gamma(e1,rad);      % Gamma function call

rad = pi/2 - rad;

for nt = 1:10
%h = 1.5;
h = 0.1*nt + .0                 % Height of antenna

% Computation of the path length difference

p2 = h/cos(rad);        % Reflected path length

p1 = p2*cos(2*rad);     % Path length of straight path after
                        % reflected path hits ground
```

```
dif = p2 - p1;              % Path length difference
                            % reflected path is dif(m) greater than straight

% Computation of reflected e-field

for i = 1:ctr
        x2(i) = tau1*exp(j*k(i)*dif);
        y2(i) = tau2*exp(j*(k(i)*dif + pi/2));
%       Ec2(i) = Eo*(x2(i)^2 + y2(i)^2)^.5;
end


% Superposition can be achieved and still account for
% phase by dotting the incoming reflected wave by the
% antennae vector effective length

fpat = (cos(.53*2*rad)^5.8);     % Field Pattern

% Assume that the antennae boresight is pointed toward the
% satellite.

% Antennae vector effective length can be computed by
% the equation on page 142 of Stutzman.  The part under
% the root sign can be set equal to .5, leaving only
% fpat.

% h(theta) = fpat(theta)x~  +- j*fpat(theta)y~

% Computation of the superposition of the two fields
% Finds the induced voltage in the antenna.

for i = 1:ctr
        xt(i) = x(i) + x2(i)*cos(2*rad)*fpat;
                % Cos factor transforms this into .
                % coordinate system of unobstructed path

        yt(i) = y(i) + y2(i)*fpat;
        Vfs(i) = Eo*(1/sqrt(2))*(x(i) + y(i));
                % Free space signal level
        Voc(i) = Eo*(2^(-.5))*(xt(i) + yt(i));
        Voc1(i) = 20*log10(Voc(i)) - 20*log10(Vfs(i)) - 5.5;
end

% Plots of Combined Paths

subplot(5,2,nt),plot(fr,Voc1);
%title('Model 2c Recieved Voc vs Transmitted Frequency (tau = 1) ');
%ylabel('Voc Magnitude (dB) ');
%xlabel('Transmitted Frequency (Hz) ');
grid;
end

gtext('Signal level  vs. Frequency')
%gtext('Figure 5.3.7 Signal level (dB) vs. Frequency (MHz) for Model 2')
%gtext('Angle scan:angle = 10 to 55 deg., height = 1.5 m')

gtext('Figure 5.3.6 Signal level (dB) vs. Frequency (MHz) for Model 2')
gtext('Height scan: angle = 18 deg., height = 0.1 to 1.0 m')
```

```
% Model 3e
% Models a circularly polarized wave incident upon a receiver
%  between two parallel plates separated by a distance b.
% Takes into account the first three reflections.
% Sattelite is said to be at infinity
% Antennae is at a fixed height and the
% frequency is swept from 700 MHz to 1.8 GHz
% Reflection coeficients of are calculated
% using the gamma.m function

clear
clf

% Eo amplitude of E-field
% This is circularly polarized so the amplitude of the vector is constant

Eo = 1;

% Constants

z = 0;                          % Arbitrary z value
c = 3e8;                        % Speed of light
b = 2.2;                        % Distance between plates

e0 = 8.854e-12;                 % Permittivity of free space
mu0 = pi*4e-7;                  % Permeability of free space

% Frequency swept from 700 MHz to 1.8 GHz

ctr = 0;                                % counter
for f = 7e8:1e6:18e8;
        ctr = ctr + 1;                  % Increment Counter
        fr(ctr) = f/1e6;                % Operating Frequency
        w(ctr) = 2*pi*f;                % Frequency in Radians
        k(ctr) = w(ctr)*(sqrt(e0*mu0));% Phase constant
end

%for nt = 1:10
ang = 16; %
%ang = 19 + .1*nt               % Elevation angle of the satellite
ang = 90 - ang;                 % Converts elevation angle to incidence
rad = ang*pi/180;               % Converts angle to radians

% Calculation of the Reflection coefficient

mu1 = mu0;
e2 = .026;
e1 = 10-j;                      % Complex permittivity of concrete
[gp,gn,tp,tn] = gamma(e1,rad);  % Gamma function call

rad = pi/2 - rad;

% Circularly polarized field equation for ray 1

for i = 1:ctr
        x(i) = exp(j*k(i)*z);
        y(i) = exp(j*(k(i)*z + pi/2));  % y 90 deg. out of phase
end
```

```
% Graphs the model for 10 different receiver heights

%for nt = 1:10
h = 1.3;
%h = 0.01*nt + 1.44                        % Height of antenna

% Computation of the path length difference

c = h/sin(rad);                  % Ray 2, 1st reflected path
d = b/sin(rad);                  % Length of path after equiphase wavefront
e = d;                           % Ray 3, 1st reflected path
g = (b-h)/sin(rad);              % Ray 3, 2nd reflected path
f2 = c*sin(pi/2 - 2*rad);
fp = e*sin(pi/2 - 2*rad);        % Ray 1 Eq.Wf. to top plate
f = g + fp;                      % Ray 1 Eq.Wf to receiver length

% Ray 1 arrives at z = 0
% Ray 2 arrives at z = c + d - f
% Ray 3 arrives at z = e + g - f

r2 = c-f2;               % Ray 2 path length difference
r3 = e+g-f;              % Ray 3 path length difference


% Computation of Ray 2 e-field

for i = 1:ctr
        x2(i) = gp*exp(j*k(i)*r2);
        y2(i) = gn*exp(j*(k(i)*r2 + pi/2));
end

% Computation of Ray 3 e-field

for i = 1:ctr
        x3(i) = gp*gp*exp(j*k(i)*r3);
        y3(i) = gn*gn*exp(j*(k(i)*r3+pi/2));
end


% Superposition can be achieved and still account for
% phase by dotting the incoming reflected wave by the
% antennae vector effective length

fpat = (cos(.53*2*rad)^5.8);     % Field Pattern

% Assume that the antenna boresight is pointed toward the
% satellite.

% Antenna vector effective length can be computed by
% the equation on page 142 of Stutzman.  The part under
% the root sign can be set equal to .5, leaving only
% fpat.

% h(theta) = fpat(theta)x~  +- j*fpat(theta)y~

% Computation of the superposition of the two fields
% Finds the induced voltage in the antenna.

for i = 1:ctr
        xt(i) = x(i) + x2(i)*cos(2*rad)*fpat + x3(i);
                % Cos factor transforms this into
```

```
                % coordinate system of unobstructed path

        yt(i) = y(i) + y2(i)*fpat + y3(i);
        Vfs(i) = Eo*(1/sqrt(2))*(x(i) + y(i));
        Voc(i) = Eo*(1/sqrt(2))*(xt(i) + yt(i));
        Voc1(i) = 20*log10(Voc(i)) - 20*log10(Vfs(i)) - 5.5;
end

% Plots of Combined Paths

%subplot(5,2,nt),
plot(fr,Voc1);
axis([700 1800 -30 5])
title('Signal level vs. Frequency');
ylabel('Voc Magnitude (dB) ');
xlabel('Transmitted Frequency (MHz) ');
grid;
%end

%gtext('Figure 6.2.3 Signal level (dB) vs. Frequency (MHz) for model 3')
%gtext('Figure 6.2.1 Height scan: 1.45 to 1.54 meters, Angle: 19.5')
%gtext('Figure 6.3.1 Match for Vogel's figure 9')
%gtext('Figure 6.2.2 Signal level (dB) vs. Frequency (MHz) for Model 3')
%gtext('Angle scan:angle = 19.1 to 20 deg., height = 1.5 m')

%gtext('Figure 6.2.1 Signal level (dB) vs. Frequency (MHz) for Model 3')
%gtext('Height scan: angle = 19.5 deg., height = 1.45 to 1.54 m')

%gtext('Height = 1.5 meters, Angle = 19.6 degrees')
```

```
% Model 3f
% Models a circularly polarized wave incident upon a receiver
%  between two parallel plates separated by a distance b.
% Takes into account the first three reflections.
% LOS path is unobstructed.
% Sattelite is said to be at infinity
% Antennae is at a fixed height and the
% frequency is swept from 700 MHz to 1.8 GHz
% Reflection coeficients of are calculated
% using the gamma.m function

clear
clf

% Eo amplitude of E-field
% This is circularly polarized so the amplitude of the vector is constant

Eo = 10;

% Constants

z = 0;                          % Arbitrary z value
c = 3e8;                        % Speed of light
b = 2.2;                                % Distance between plates

e0 = 8.854e-12;                 % Permittivity of free space
mu0 = pi*4e-7;                  % Permeability of free space

% Frequency swept from 700 MHz to 1.8 GHz

ctr = 0;                                % counter
for f = 7e8:1e6:18e8;
        ctr = ctr + 1;          % Increment Counter
        fr(ctr) = f/1e6;                % Operating Frequency
        w(ctr) = 2*pi*f;                % Frequency in Radians
        k(ctr) = w(ctr)*(sqrt(e0*mu0));% Phase constant
end
%for nt = 1:10
ang = 16; %
%ang = 17.5 + .1*nt             % Elevation angle of the satellite
ang = 90 - ang;                 % Converts elevation angle to incidence
rad = ang*pi/180;       % Converts angle to radians

% Calculation of the Reflection coefficient

mu1 = mu0;
e2 = .026;
e1 = 10-j;                      % Complex permittivity of concrete
[gp,gn,tp,tn] = gamma2(e1,rad); % Gamma function call

rad = pi/2 - rad;

% Circularly polarized field equation for ray 1

for i = 1:ctr
        x(i) = exp(j*k(i)*z)/.5309;
        y(i) = exp(j*(k(i)*z + pi/2))/.5309;    % y 90 deg. out of phase
end
```

```
% Graphs the model for 10 different receiver heights

%for nt = 1:10
h = 1.3;
%h = 0.1*nt + 0.2                          % Height of antenna
% changing the receiver height doesn't change where the
% nulls occur, it just changes which ones are accented
% Best null positioning occurs with h = .3 & ang = 30
% for a room of height 2.3 matches fig 5

% Computation of the path length difference

c = h/sin(rad);          % Ray 2, 1st reflected path
d = b/sin(rad);          % Length of path after equiphase wavefront
e = d;                   % Ray 3, 1st reflected path
g = (b-h)/sin(rad);      % Ray 3, 2nd reflected path
f2 = c*sin(pi/2 - 2*rad);
fp = e*sin(pi/2 - 2*rad); % Ray 1 Eq.Wf. to top plate
f = g + fp;              % Ray 1 Eq.Wf to receiver length

% Ray 1 arrives at z = 0
% Ray 2 arrives at z = c + d - f
% Ray 3 arrives at z = e + g - f

r2 = c-f2;               % Ray 2 path length difference
r3 = e+g-f;              % Ray 3 path length difference


% Computation of Ray 2 e-field

for i = 1:ctr
        x2(i) = gp*exp(j*k(i)*r2);
        y2(i) = gn*exp(j*(k(i)*r2 + pi/2));
end

% Computation of Ray 3 e-field

for i = 1:ctr
        x3(i) = gp*gp*exp(j*k(i)*r3);
        y3(i) = gn*gn*exp(j*(k(i)*r3+pi/2));
end


% Superposition can be achieved and still account for
% phase by dotting the incoming reflected wave by the
% antennae vector effective length

fpat = (cos(.53*2*rad)^5.8);     % Field Pattern

% Assume that the antenna boresight is pointed toward the
% satellite.

% Antenna vector effective length can be computed by
% the equation on page 142 of Stutzman.  The part under
% the root sign can be set equal to .5, leaving only
% fpat.

% h(theta) = fpat(theta)x~  +- j*fpat(theta)y~

% Computation of the superposition of the two fields
% Finds the induced voltage in the antenna.
```

```
for i = 1:ctr
        xt(i) = x(i) + x2(i)*cos(2*rad)*fpat + x3(i);
                % Cos factor transforms this into
                % coordinate system of unobstructed path

        yt(i) = y(i) + y2(i)*fpat + y3(i);
        Vfs(i) = Eo*(1/sqrt(2))*(x(i) + y(i));
        Voc(i) = Eo*(1/sqrt(2))*(xt(i) + yt(i));
        Voc1(i) = 20*log10(Voc(i)) - 20*log10(Vfs(i));

end

% Plots of Combined Paths

%subplot(2,1,1),
plot(fr,Voc1);
axis([700 1800 -30 5])
%title(' MODEL 3f Proposed fit to fig. 10 (h = 1.3 angle = 16.0 degrees) ');
title('Signal level  vs. Frequency')

ylabel('Voc Magnitude (dB) ');
xlabel('Transmitted Frequency (MHz) ');
grid;
end

%gtext('Figure 6.3.2 Match for Vogel's figure 10')
```

```
% Power Delay Profile of model3c

clear

e0 = 8.854e-12;                 % Permittivity of free space
mu0 = pi*4e-7;                  % Permeability of free space

f = 700e6;
w = 2*pi*f;                % Frequency in Radians
k = w*(sqrt(e0*mu0));% Phase constant


z = 0;                          % Arbitrary z value
c = 3e8;                        % Speed of light
b = 2.2;                        % Distance between plates

ang = 18;                % Elevation angle of the satellite
ang = 90 - ang;          % Converts elevation angle to incidence
rad = ang*pi/180;        % Converts angle to radians

mu1 = mu0;
e2 = .026;
e1 = 10-j;               % Complex permittivity of concrete
[gp,gn,tp,tn] = gamma(e1,rad);  % Gamma function call

rad = pi/2 - rad;

h = 1.5;

c = h/sin(rad);          % Ray 2, 1st reflected path
d = b/sin(rad);          % Length of path after equiphase wavefront
e = d;                   % Ray 3, 1st reflected path
g = (b-h)/sin(rad);      % Ray 3, 2nd reflected path
f2 = c*sin(pi/2 - 2*rad);
fp = e*sin(pi/2 - 2*rad); % Ray 1 Eq.Wf. to top plate
f = g + fp;              % Ray 1 Eq.Wf to receiver length

% Ray 1 arrives at z = 0
% Ray 2 arrives at z = c + d - f
% Ray 3 arrives at z = e + g - f

r2 = c-f2;               % Ray 2 path length difference
r3 = e+g-f;              % Ray 3 path length difference


c = 3e8;                 % Speed of Light

tr(1) = 0;               % Ray 1 arrives first
tr(2) = r2/c;            % Ray 2 time difference
tr(3) = r3/c;            % Ray 3 time difference
tr = tr*1e9;
% Calculation of respective electric fields

x = exp(j*k*z);
y = exp(j*k*z);

x2 = gp*exp(j*k*r2);
y2 = gn*exp(j*(k*r2 + pi72));

x3 = gp*gp*exp(j*k*r3);
```

```
y3 = gn*gn*exp(j*(k*r3 + pi/2));

% Calculation of respective power

eta = sqrt(mu0/e0);
c1 = 1/(2*eta);
p(1) = c1*(real(x).^2 + real(y).^2);
p(2) = c1*(real(x2).^2 + real(y2).^2);
p(3) = c1*(real(x3).^2 + real(y3).^2);

pt = p(1) + p(2) + p(3);

pp(1) = p(1)/pt;
pp(2) = (p(1) + p(2))/pt;
pp(3) = (p(1) + p(2) + p(3))/pt;
pp = pp*100;

plot(tr,pp)
axis([0 5 0 100])
title('Power Delay Profile')
xlabel('Time (nanoseconds) ')
ylabel('Percentage of Total Power')
gtext('Figure 6.4.1 Power delay profile')

% Calculation of Mean Excess Delay
```